

AD-A285 791



NPSEC-94-013

NAVAL POSTGRADUATE SCHOOL
Monterey, California



94-33339



Wavelet Time-Frequency Analysis
of Phase-Shift-Key Modulated Signals

by

Alex W. Lam

September 29, 1994

Approved for public release; distribution unlimited.

Prepared for: Naval Research Laboratory

94 10 27 05 1

Naval Postgraduate School
Monterey, California 93943-5000

Rear Admiral T. A. Mercer
Superintendent

H. Shull
Provost

This report was funded by the Naval Research Laboratory.

Approved for public release; distribution unlimited.

This report was prepared by:



ALEX W. LAM
Associate Professor,
Department of Electrical and
Computer Engineering

Reviewed by:

Released by:



MICHAEL A. MORGAN
Chairman,
Department of Electrical and
Computer Engineering



PAUL J. MARTO
Dean of Research

Purpose: Reporting burden for this collection of information is estimated to average 1 hour per response, including the time for reviewing instructions, searching existing data sources, gathering and maintaining the data needed, and completing and reviewing the collection of information. Send comments regarding this burden estimate or any other aspect of this collection of information, including suggestions for reducing the burden, to Washington Headquarters Services, Directorate for Information Operations and Reports, 1215 Jefferson Davis Highway, Suite 1204, Arlington, VA 22202-4302, and to the Office of Management and Budget, Paperwork Reduction Project (0704-0188), Washington, DC 20503.

1. AGENCY USE ONLY (Leave blank)		2. REPORT DATE September 29, 1994	3. REPORT TYPE AND DATES COVERED Final Report Oct 1, 1993-Sep 30, 1994	
4. TITLE AND SUBTITLE Wavelet Time-Frequency Analysis of Phase-Shift-Key Modulated Signals			5. FUNDING NUMBERS	
6. AUTHOR(S) Alex W. Lam				
7. PERFORMING ORGANIZATION NAME(S) AND ADDRESS(ES) Naval Postgraduate School Monterey, CA 93943-5000			8. PERFORMING ORGANIZATION REPORT NUMBER NPSEC-94-013	
9. SPONSORING/MONITORING AGENCY NAME(S) AND ADDRESS(ES) Naval Research Laboratory Washington, DC 20375-5320			10. SPONSORING/MONITORING AGENCY REPORT NUMBER	
11. SUPPLEMENTARY NOTES The views expressed in this report are those of the authors and do not reflect the official policy or position of the Department of Defense or the United States Government.				
12a. DISTRIBUTION/AVAILABILITY STATEMENT Approved for public release; distribution unlimited.			12b. DISTRIBUTION CODE	
13. ABSTRACT (Maximum 200 words) Continuous and discrete wavelet transforms are discussed. Recursive generations of compactly supported wavelet time functions are described. Haar, Daubechies, and complex modulated Gaussian wavelets are utilized to analyze phase shifts in signals with noise.				
14. SUBJECT TERMS wavelet transform, multi-resolution time-frequency analysis, phase-shift-key, compactly supported wavelets, Gaussian wavelets			15. NUMBER OF PAGES 62	
			16. PRICE CODE	
17. SECURITY CLASSIFICATION OF REPORT UNCLASSIFIED	18. SECURITY CLASSIFICATION OF THIS PAGE UNCLASSIFIED	19. SECURITY CLASSIFICATION OF ABSTRACT UNCLASSIFIED	20. LIMITATION OF ABSTRACT SAR	

**WAVELET TIME-FREQUENCY ANALYSIS
OF
PHASE-SHIFT-KEY MODULATED SIGNALS**

Alex W. Lam

Department of Electrical and Computer Engineering
Naval Postgraduate School
Monterey, CA 93943

Technical Report
September 1994



A-1

ABSTRACT

Continuous and discrete wavelet transforms are discussed. Recursive generations of compactly supported wavelet time functions are described. Haar, Daubechies, and complex modulated Gaussian wavelets are utilized to analyze phase shifts in signals with noise.

Keywords: Wavelet transform, multiresolution time–frequency analysis, phase–shift–key, compactly supported wavelets, complex modulated Gaussian wavelets.

TABLE OF CONTENT

1.	INTRODUCTION	3
2.	CONTINUOUS WAVELET TRANSFORM	4
3.	DISCRETE WAVELET TRANSFORM	10
3.1	Orthonormal Wavelet Decomposition	10
3.2	Discrete Wavelet Transform	13
3.3	Wavelet Conditions and Generations	15
3.3.1	Wavelet conditions	15
3.3.2	Generation of wavelet function	17
3.3.3	Compactly supported wavelets examples	20
3.4	Multiple-Phase Discrete Wavelet Transform	27
4.	DETECTION OF PSK SIGNALS	30
4.1	Rectangular Wave	30
4.1.1	Haar wavelet	30
4.1.2	Daubechies wavelet	35
4.1.3	Complex modulated Gaussian wavelet	39
4.2	180° Phase Shift	5
5.	CONCLUDING REMARKS	5
	REFERENCES	1

1. INTRODUCTION

We have investigated several time-frequency decomposition techniques and their applications in the detection and analysis of digitally modulated signals [10], [14], [13]. In this report, we will specifically discuss wavelet decompositions and present a few preliminary results.

The one particular digital modulation that we consider in here is binary phase-shift-key (BPSK) signal, which is a sinusoid modulated by a baseband rectangular data waveform. Over a duration of one binary data bit, the phase of a BPSK wave is either 0° or 180° depending on the value of the data, which is either +1 or -1. For example, a wave with data rate 9600 bps can change phase every $1/9600$ seconds. In tactical communications using direct-sequence spread-spectrum (DS/SS) [11], the corresponding spread BPSK wave can change phase N times faster, where N is the spectrum spreading factor. Since BPSK and its extensions (such as QPSK and OQPSK) are the most predominant modulation formats used in practice, there are interests in developing efficient methods for detecting the phase shifts under various channel and noise scenarios. Previous research efforts have used cyclostationarity [6] and ambiguity function with specific kernel as the smoothing function [23], [13].

In Chapter 2, we will discuss the so-called continuous wavelet transform (CWT). In Chapter 3, we will discuss the discrete wavelet transform (DWT) and the computations of orthonormal compactly supported scaling and wavelet functions on the dyadic numbers. In Chapter 4, we use the wavelet time-frequency decomposition techniques to detect $\pm 180^\circ$ phase shifts in noise. A few concluding remarks are given in Chapter 5.

2. CONTINUOUS WAVELET TRANSFORM

The continuous wavelet transform (CWT) of a $L^2(\mathbb{R})$ signal $x(t)$ is defined as [8], [2], [3]:

$$X(t, a) = \frac{1}{\sqrt{a}} \int_{-\infty}^{\infty} x(u) \psi^*\left(\frac{u-t}{a}\right) du \quad (2.1)$$

where $\psi(t)$ is the *wavelet* function, " * " denotes complex conjugation, and $a > 0$. The scaling factor "a" in (2.1) is taken to be power of 2 in this report, i.e., $a = 2^{-m}$, for $m = 0, 1, 2, 3, \dots$. The inverse transform is given by:

$$x(t) = \frac{1}{c_\psi} \iint X(v, a) \frac{1}{\sqrt{a}} \psi\left(\frac{t-v}{a}\right) \frac{da dv}{a^2} \quad (2.2)$$

where the constant

$$c_\psi = \int |\Psi(f)|^2 \frac{df}{|f|} \quad (2.3)$$

must be finite. This implies that the wavelet function must satisfy

$$\Psi(f) = 0, \quad \text{i.e.,} \quad \int \psi(t) dt = 0 \quad (2.4)$$

Thus, the wavelet function is bandpass type with Fourier transform $\Psi(f) = 0$ at $f = 0$; equivalently, the area under the wavelet function is exactly 0. Note that we can rewrite (2.1) as

$$X(t, a) = \sqrt{a} \int X(f) \Psi^*(af) \exp(j2\pi ft) df \quad (2.5)$$

in terms of the Fourier transforms. The CWT can be computed via (2.1) or (2.5).

The CWT $X(t, a)$ represents a decomposition of $x(t)$ into a time-scale plane. Usually, $X(t, a)$ is graphed against time t and the log scale $\log_2(a)$. The CWT can be regarded as a constant-Q bandpass filter since (2.1) is a convolution of two time functions. The linear bandpass filter impulse response at level m is

$$\Psi_m(t) = 2^{m/2} \psi^*(2^m t) \quad (2.6)$$

If we define " f_m " as the r.m.s. center frequency of the passband by

$$\int_0^{\infty} (f - f_m)^2 |\Psi_m(f)|^2 df = 0 \quad (2.7)$$

then we have

$$f_m = 2^m f_0 \quad \text{and} \quad \sigma_m = 2^m \sigma_0 \quad (2.8)$$

where f_0 is the r.m.s. center frequency and $2\sigma_0$ is the r.m.s. bandpass bandwidth of the *basic* wavelet function $\psi(t)$. The ratio of f_m to σ_m is always equal to

$$\frac{f_m}{\sigma_m} = \frac{f_0}{\sigma_0} \quad (2.9)$$

which is constant for all decomposition level m . As the level of decomposition (i.e., m) increases, the filtering function $\psi_m(t)$ of (2.6) becomes narrower in time. The time resolution of the wavelet decomposition therefore increases with m . On the other hand, the r.m.s. bandpass bandwidth (i.e., $2\sigma_m$) of $\psi_m(t)$ increases exponentially with m , and therefore the frequency-resolution of the wavelet decomposition is better for smaller m . Unlike the classical time-frequency transforms such as the short-time Fourier transform (STFT) or the Gabor transform (GT) [1], [9], which do not scale the filtering function and have constant time-resolution at all frequencies, the wavelet transform has higher time-resolution at higher frequency. One can observe that for CWT, its time-resolution is increasingly better at higher frequencies, while its frequency-resolution is increasingly better at lower frequencies.

We will use the complex modulated Gaussian wavelet function:

$$\begin{aligned} \psi(t) &= \exp(j2\pi f_\psi t) \exp(-t^2/2\sigma^2) \\ &= \cos 2\pi f_\psi t \exp(-t^2/2\sigma^2) + j \sin 2\pi f_\psi t \exp(-t^2/2\sigma^2) \end{aligned} \quad (2.10)$$

Of course the Fourier transform of a Gaussian function is a Gaussian function, and the complex exponential time function $\exp(j2\pi f_\psi t)$ will cause a shift by f_ψ in frequency in the Fourier transform. It is then possible to choose f_ψ big enough so that for complex modulated Gaussian wavelet we have

$$\Psi(f) = 0 \quad \text{for } f < 0 \quad (2.11)$$

Condition (2.11) is especially desirable when the wavelet is used to analyze sinusoids. For example, let $x(t) = \cos 2\pi f_c t$, for t in a very large, yet finite, window. Using (2.5), we have

$$X(t, a) = \frac{\sqrt{a}}{2} \exp(j2\pi f_c t) \Psi^*(af_c) + \frac{\sqrt{a}}{2} \exp(-j2\pi f_c t) \Psi^*(-af_c) \quad (2.12)$$

If $\Psi(f)$ satisfy (2.11), then the second term in (2.12), which is a contribution by the impulse $\delta(f+f_c)$, drops out. It follows that the phase of the resulting CWT $X(t, a)$ will nicely reveal the center frequency of the carrier wave $x(t) = \cos 2\pi f_c t$. For other stationary or non-stationary signals, magnitude and phase of $X(t, a)$, with $\psi(t)$ being the complex Gaussian wavelet, will reveal the frequency as well as the time behaviors of the signal.

We also remark that we can multiply a suitable baseband function $b(t)$ with the complex sinusoid $\exp(j2\pi f_\psi t)$ to obtain a wavelet function:

$$\psi(t) = \exp(j2\pi f_\psi t) b(t) \quad (2.13)$$

so that its Fourier transform is zero on the negative frequency axis. The above construction yields a large class of potentially useful wavelet functions. The preference to use the Gaussian envelope $\exp(-t^2/2\sigma^2)$ is due to the fact that the Gaussian function achieves the lower bound in the uncertainty principle:

$$\Delta t \Delta f \geq \frac{1}{4\pi} \quad (2.14)$$

with equality, where Δt is the r.m.s. time-spread and Δf is the r.m.s. frequency-spread of the signal [20]. Note that two pulses in time can be discriminated only if they are more than Δt seconds apart in time, and two sinusoids can be discriminated only if they are more than Δf apart in frequency. Equation (2.14) states that one can only trade time-resolution for frequency-resolution, or vice versa.

Using CWT, the frequency-resolution Δf is in the order of $\sigma_m = 2^m \sigma_0$. Viewing the CWT $X(t, a)$ in a time-scale plane allow us to look at the signal at different scale (i.e., different frequencies in the passband of $2\sigma_m$ Hz wide around the center frequency f_m). The CWT indeed presents a multiresolutional analysis of the signal, as if the signal is being processed by a bank of filters with logarithmically spaced centered frequency f_m but constant bandwidth to frequency ratio of $2\sigma_m/f_m = 2\sigma_0/f_0$. These relationships are best visualized by considering the complex modulated sinc wavelet function:

$$\psi(t) = \exp(j2\pi f_\psi t) \frac{1}{\sqrt{W}} \operatorname{sinc} \frac{t}{W} \quad (2.15)$$

which has a rectangular passband with bandwidth equal to $2\sigma_0 = W$. The center frequency of $\psi(t)$ is exactly equal to f_ψ . We also propose to use this complex modulated sinc wavelet to analyze our signals.

Computation of $X(t, a)$ could be lengthy and expensive. In practice, however, we only have a finite-length sampled sequence: $x(nT)$, $n = 0, 1, 2, \dots, N_s - 1$, where N_s is the sequence length and the sampling rate is at least equal to the Nyquist rate, which is twice the highest frequency component in the signal $x(t)$. We will only compute $X(t, a)$ at the sampling times $t = nT$ and at levels $m = 0, 1, 2, \dots, [\log_2 N_s]$. The integral of (2.1) is now reduced to a finite summation and the computation burden is greatly relieved. In this discrete-time approximation of the CWT, we essentially perform a multiresolutional analysis of an *auxiliary* signal $x_a(t)$, which is a piecewise linear function constructed by joining two consecutive sampled points $x(nT)$ and $x((n+1)T)$ with a straight line. Towards this end, the CWT of (2.1) produces a total of $N_{\max} = [\log_2 N_s] + 1$ snap-shots of the auxiliary signal via bandpass filterings.

The complex modulated Gaussian wavelet of (2.10) is a nice analytical function. It is continuous and differentiable everywhere. Perhaps one drawback is that it has an infinitely span and therefore it is not a causal filter impulse response. In practice, however, this mishap can be resolved by using a wavelet with sufficiently fast decay over the processing window so that it can be regarded as of finite span. We select the Gaussian wavelet because of two additional reasons: (a) tunability; and (b) bandwidth adjustability. By varying the modulating frequency f_ψ , we can place the passband anywhere on the frequency axis. Second, by altering σ , the bandwidth of the wavelet function $\psi(t)$ can be selected at will. Each (f_ψ, σ) selection will result in a multiresolutional analysis that consists of N_{\max} snap-shots of the signal. A systematic selection of (f_ψ, σ) will allow a thorough analysis of the signal at all possible time-resolution and frequency-resolution levels.

We show an example of a complex modulated Gaussian wavelet function $\psi(t)$ with $f_\psi = 8$ Hz and $\sigma = 0.12$ in Figure 2.1. This value is selected so that all the energy in the wavelet is essentially contained in the compact time interval $[-0.5, 0.5]$ for presentation purpose. In the left column of Figure 2.1, the real part, imaginary part, magnitude, and phase of the wavelet are depicted. In the right column, the energy spectral densities (which is magnitude square of the Fourier transform) of the real part, imaginary part, and the wavelet function itself are shown. Note that this complex wavelet has no spectral component in the negative frequency axis, a desirable property as discussed previously. The spectrum is centered around $f = f_\psi = 8$ and the r.m.s. passband bandwidth of $\psi(t)$ is $2\sigma = 0.24$. In processing a given signal $x(t)$, the signal is first

normalized to be contained in the time interval $[0, 1]$; it is then decomposed by the analyzing functions $\psi_m(t)$, with $\psi_0(t) = \psi(t)$ contained also in the interval $[0, 1]$.

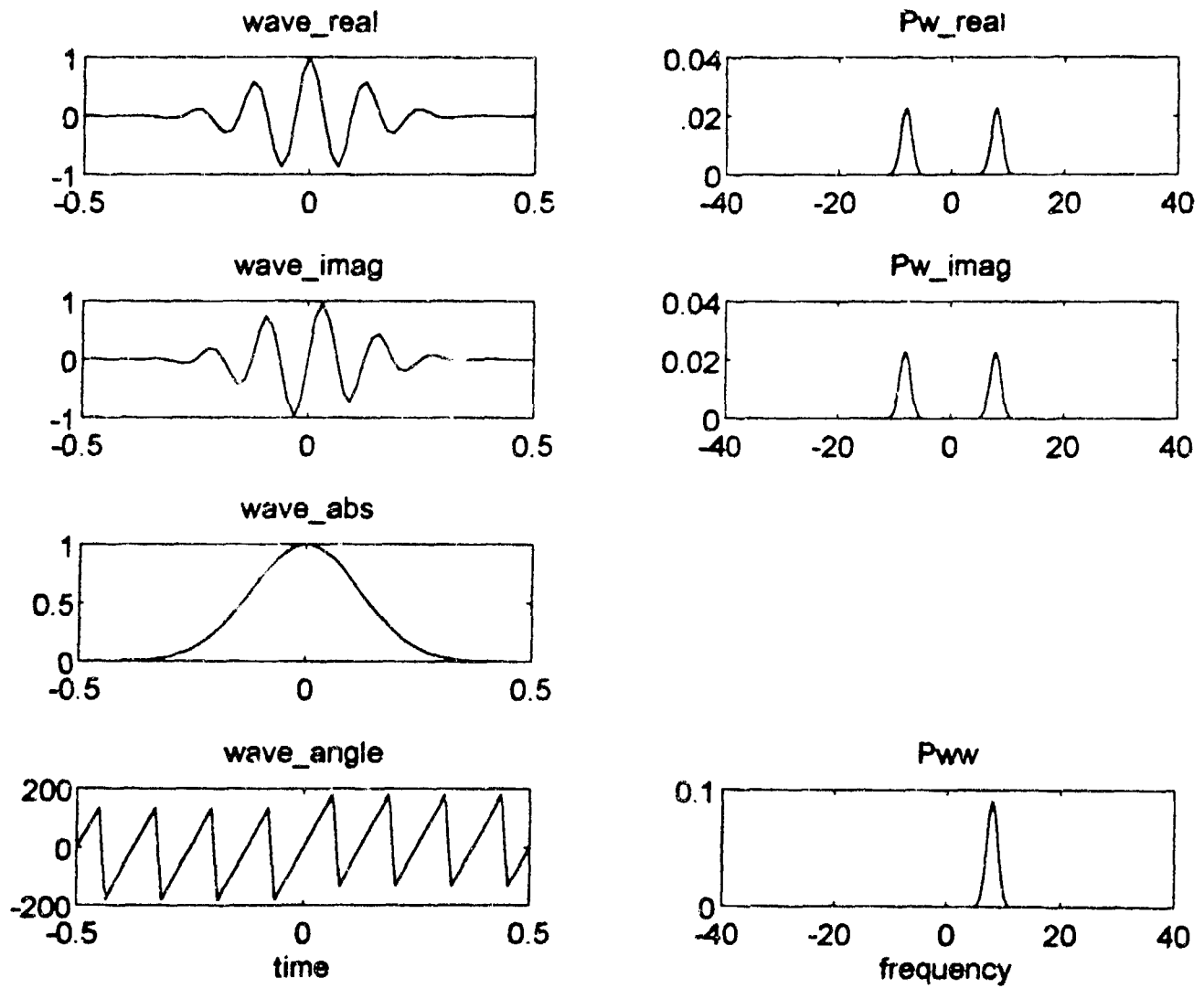


Fig. 2.1 Complex modulated Gaussian wavelet function $\psi(t)$: time-domain functions and energy spectral densities. $f_\psi = 8$, $\sigma = 0.12$.

3. DISCRETE WAVELET TRANSFORM

In this section we will discuss an orthonormal decomposition of a signal $x(t)$ using a scaling/wavelet function pair, and describe the so-called discrete wavelet transform (DWT) algorithm using orthonormal wavelet functions [4], [16], [17], [18]. We will also discuss the multiple-phase DWT, and generations of wavelet functions that have compact (i.e., closed and bounded) support.

3.1 Orthonormal Wavelet Decomposition

Consider a nested sequence of closed subspaces $\{V_m; m \in \mathbb{Z}\}$ in $L^2(\mathbb{R})$ such that

$$\{0\} = \dots \subset V_{-2} \subset V_{-1} \subset V_0 \subset V_1 \subset V_2 \subset \dots = L^2(\mathbb{R}) \quad (3.1)$$

where $\bigcap_{m \in \mathbb{Z}} V_m = \{0\}$ and $\overline{\bigoplus_{m \in \mathbb{Z}} V_m} = L^2(\mathbb{R})$. One can find an unique scaling

(or averaging) function $\phi(t)$ such that $\{\phi_{m,n}(t); n \in \mathbb{Z}\}$ is an orthonormal basis of V_m where

$$\phi_{m,n}(t) = \alpha^{m/2} \phi(\alpha^m t - nT) \quad (3.2)$$

by normalizing, dilating or contracting, and time-shifting $\phi(t)$. The value of $T (>0)$ is arbitrary. As is common in dyadic multiresolution analysis, we take $\alpha (\neq 0,1)$ to be 2 in this report.

The orthogonal projection of a finite-energy deterministic function, $x(t)$, onto the subspace V_m is an approximation of that function at resolution level m . We can write:

$$x_m(t) = \sum_{n \in \mathbb{Z}} b_{m,n} \phi_{m,n}(t)$$

where

$$b_{m,n} \equiv \langle x(t), \phi_{m,n}(t) \rangle \equiv \int_{-\infty}^{\infty} x(t) \phi_{m,n}^*(t) dt = (x * \phi_{m,0}^*)(n2^{-m}T) \quad (3.3)$$

is a coefficient equal to the orthogonal projection of $x(t)$ onto the basis function $\phi_{m,n}(t)$. Here, $\bar{x}(t) = x(-t)$. Since $\{V_m\}$ is a sequence of dense and nested subspaces, we have $x_m(t) \rightarrow x(t)$ in

$\mathbb{L}^2(\mathbb{R})$ as $m \rightarrow \infty$. By dilating (when $m < 0$) or contracting ($m > 0$) the scaling function, approximation for $x(t)$ at any resolution level can be obtained by increasing the number of coefficients exponentially with m . Although the set of functions $\{\phi_{m,n}(t); (m, n) \in \mathbb{Z}^2\}$ spans the entire space $\mathbb{L}^2(\mathbb{R})$, it is not a minimal set because the subspaces $\{V_m\}$ are nested; in particular, $\phi_{m,n}(t)$ and $\phi_{\ell,k}(t)$ are correlated for $m \neq \ell$. For many applications, for example in image processing and compact coding, it is desirable to construct an orthonormal multiresolution basis for $\mathbb{L}^2(\mathbb{R})$. Towards this end, let $V_m = V_{m-1} \oplus W_{m-1}$, where W_{m-1} is the orthogonal complement of V_{m-1} in V_m . Consider V_0 with $\{\phi(t-nT); n \in \mathbb{Z}\}$ as its orthonormal basis. One can construct a *wavelet* function $\psi(t)$ from $\phi(t)$ so that $\{\psi(t-nT); n \in \mathbb{Z}\}$ is an orthonormal basis for W_0 ; furthermore, $\{\psi_{m,n}(t); n \in \mathbb{Z}\} = \{2^{m/2}\psi(2^m t - nT); n \in \mathbb{Z}\}$ is an orthonormal basis for W_m , and the entire set $\{\psi_{m,n}(t); (m, n) \in \mathbb{Z}^2\}$ is an orthonormal multiresolution basis for $\mathbb{L}^2(\mathbb{R})$. The relationship between the subspaces V_s and W_s is depicted in Fig. 3.1.

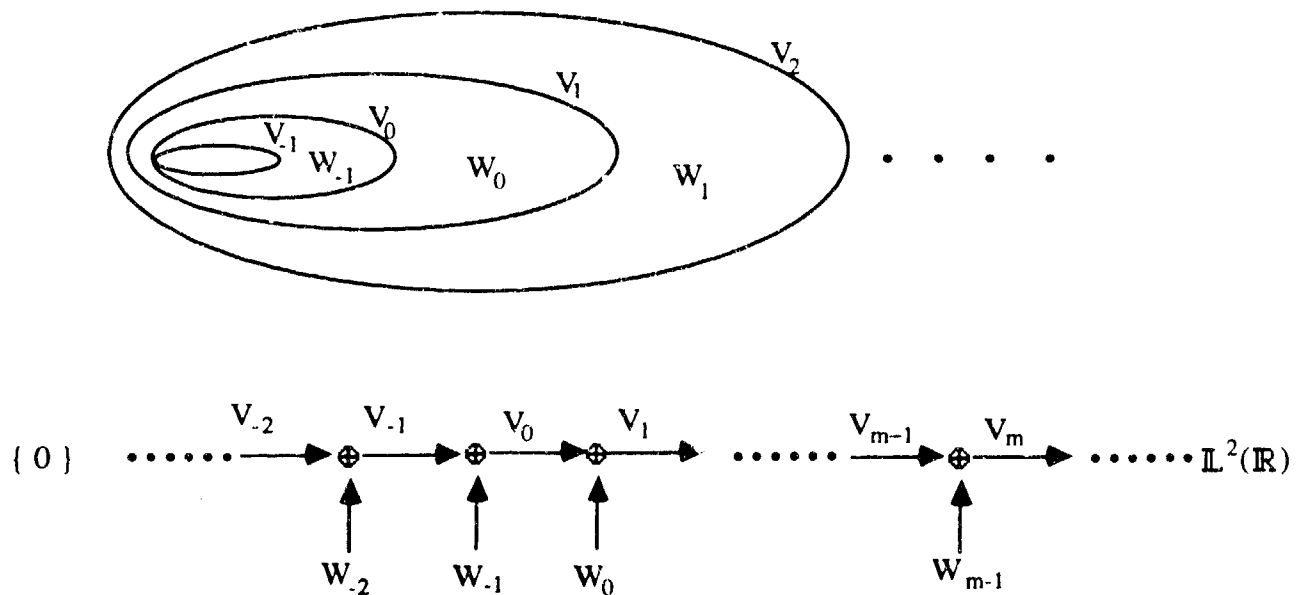


Figure 3.1 Subspaces V_s and W_s .

The orthogonal projection of $x(t)$ onto the subspace W_m is the detail function at resolution level m :

$$\begin{aligned} d_m(t) &= \sum_{n \in \mathbb{Z}} d_{m,n} \psi_{m,n}(t), \\ &= x_{m+1}(t) - x_m(t), \end{aligned} \quad d_{m,n} = \langle x(t), \psi_{m,n}(t) \rangle \quad (3.4)$$

This detail function constitutes the difference between the approximation function of $x(t)$ at resolution level $m+1$ and resolution level m . Thus, the coefficients $\{b_{m,n}; n \in \mathbb{Z}\}$ capture the information about $x(t)$ at resolution level m ; while the coefficients $\{d_{m,n}; n \in \mathbb{Z}\}$ capture the detail information going from resolution level m to resolution level $m+1$. Note that $\mathbb{L}^2(\mathbb{R}) = \bigoplus_{m \in \mathbb{Z}} W_m$ and the W s are mutually orthogonal subspaces. The sequences $\{b_{m,n}; n \in \mathbb{Z}\}$ and $\{d_{m,n}; n \in \mathbb{Z}\}$ can be obtained directly through linear filtering of $x(t)$ and then sample at time $t = n2^{-m}T$ (Fig. 3.2). Note that $\mathcal{F}[\phi_{m,0}^*(-t)]$ yields a lowpass transfer function, while $\mathcal{F}[\psi_{m,0}^*(-t)]$ is bandpass.

The wavelet decomposition filters $\psi_{m,0}^*(-t)$ can be interpreted as a parallel bank of bandpass filters (with overlapping passbands for adjacent resolution levels) that have constant size passband on the logarithm scale.

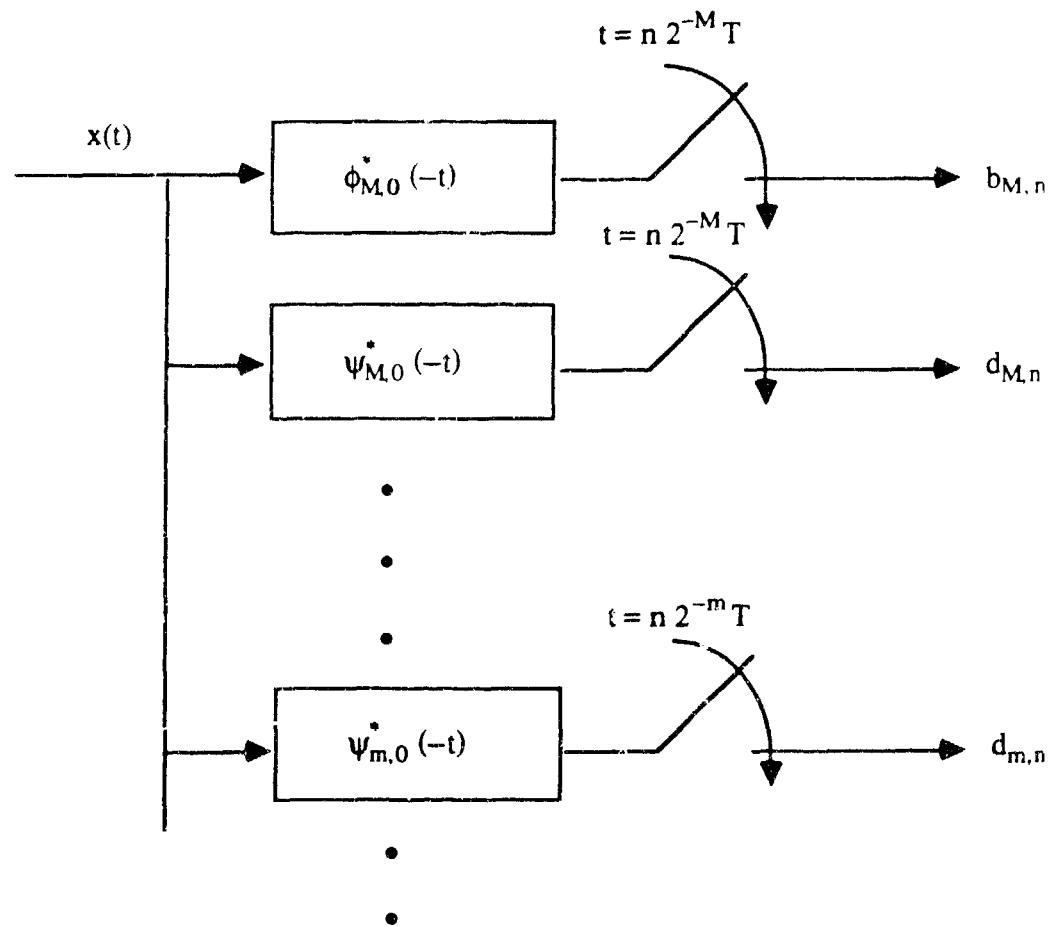


Figure 3.2 Orthonormal wavelet decomposition of the signal $x(t)$.

3.2 Discrete Wavelet Transform

There exist recursive (pyramidal) algorithms that efficiently compute the lower resolution level coefficients $\{b_{\ell,n}; n \in \mathbb{Z}\}$ and $\{d_{\ell,n}; n \in \mathbb{Z}\}$ from the higher resolution level coefficients $\{b_{m,n}; n \in \mathbb{Z}\}$, $\ell < m$; conversely, the bs at the higher resolution level m can be computed from the bs at a base (lowest) resolution level M and all the ds at lower resolution levels ℓ , $M \leq \ell < m$. These pyramidal algorithms are the so-called discrete wavelet transform (DWT) and they are described by the block diagrams in Fig. 3.3.

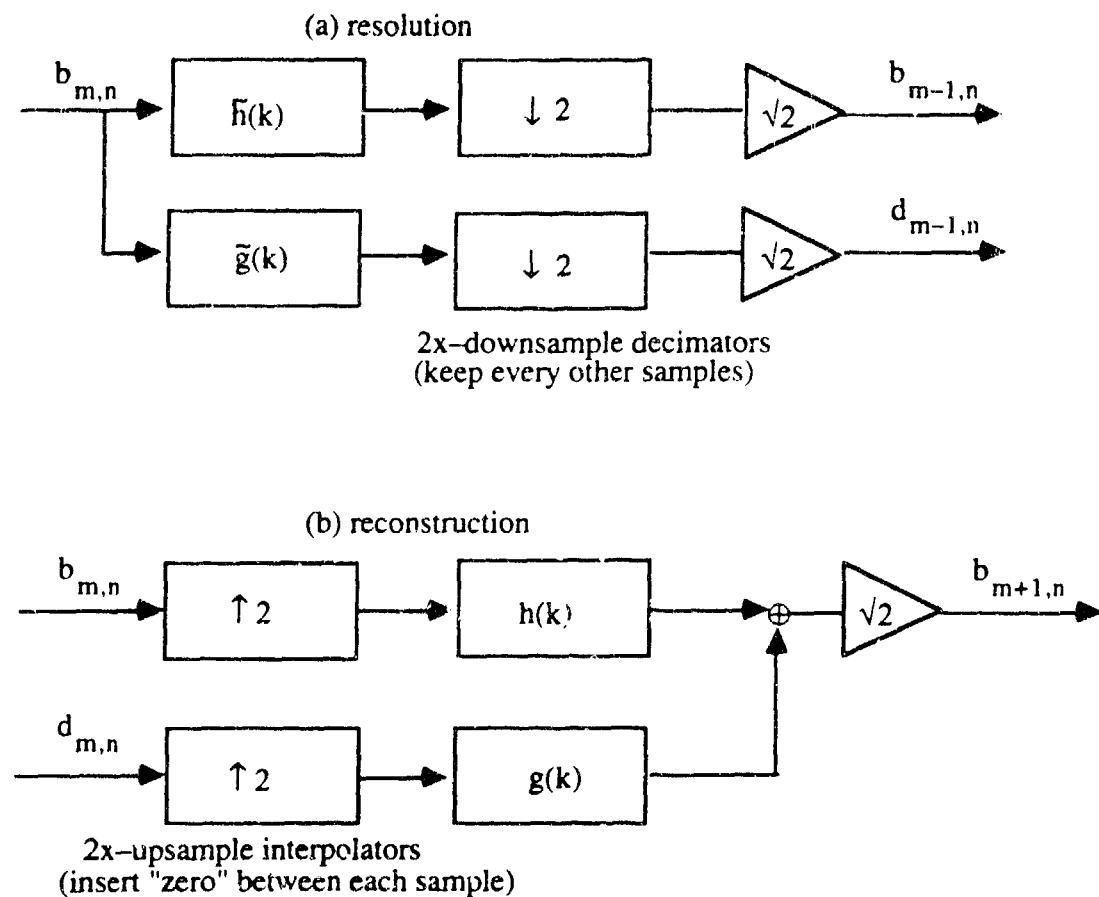


Figure 3.3 Discrete wavelet transform.

In Fig. 3.3, $h(k)$ is the impulse response of a discrete-time conjugate filter that satisfies

$$|H(\omega T)|^2 + |H(\omega T + \pi)|^2 = 1 \quad (3.5)$$

and $g(k)$ is the impulse response of the mirror filter of H with

$$G(\omega) = \exp(-j\omega) H^*(\omega + \pi) \quad (3.6a)$$

and $H(\omega T)G^*(\omega T) + H(\omega T + \pi)G^*(\omega T + \pi) = 0$ (3.6b)

One common choice of $g(n)$ that satisfies (3.6) is $g(n) = (-1)^{1-n} h(1-n)$. The scaling function and the wavelet function are orthogonal to each other and they are related by

$$\begin{aligned} \Phi(2\omega) &= H(\omega) \Phi(\omega) \\ \Psi(2\omega) &= G(\omega) \Phi(\omega) \end{aligned} \quad (3.7)$$

It follows that $\Phi(\omega) = \prod_{m=1}^{\infty} H(2^{-m}\omega)$; depending on the choice of $H(\omega)$, it is possible to obtain scaling function $\phi(t)$ that has good localization properties in both the frequency and the spatial domain. The properties of H and G in Mallat's pyramidal algorithms can be derived without reference to the multiresolution analysis [2].

Knowing the approximation function $x_M(t)$ and all the detail functions $d_\ell(t)$ at resolution level $\ell = M, M+1, M+2, \dots, m-2, m-1$, is necessary and sufficient to construct the approximation function $x_m(t)$. The approximation of $x(t)$ at resolution level m can be written as

$$x_m(t) = \sum_{n \in \mathbb{Z}} b_{m,n} \phi_{m,n}(t) = \sum_{n \in \mathbb{Z}} b_{M,n} \phi_{M,n}(t) + \sum_{M \leq \ell < m} \sum_{n \in \mathbb{Z}} d_{\ell,n} \psi_{\ell,n}(t) \quad (3.8)$$

for any $M \leq m$. Without loss of generality (WLOG), one may set $M = 0$ and $\phi(t) = \phi_{0,0}(t)$ (the lowest resolution function physically realizable), and consider resolution level $0 \leq m \leq m_{\max}$. In this report, we leave M as an arbitrary integer. An example pair for ϕ and ψ is the indicator function on $[0, T)$ and the Haar wavelet on $[0, T)$:

$$\phi(t) = \begin{cases} 1/\sqrt{T} & , 0 \leq t < T \\ 0 & , \text{otherwise} \end{cases} \quad \psi(t) = \begin{cases} 1/\sqrt{T} & , 0 \leq t < T/2 \\ -1/\sqrt{T} & , T/2 \leq t < T \end{cases} \quad (3.9)$$

In general, $\int_{-\infty}^{\infty} \phi(t) dt = \Phi(0) = \sqrt{T}$, $\Phi(\pm\infty) = 0$, and $\int_{-\infty}^{\infty} \psi(t) dt = \Psi(0) = 0$; the scaling function $\phi(t)$ can be interpreted as a lowpass function while $\psi(t)$ is bandpass. The Haar wavelet forms the only orthonormal basis of compactly supported wavelets for which the associated scaling function ϕ has a symmetry axis. Also note that the Haar wavelet is not continuous so a small error in the coefficients may cause a large fluctuation in the representation. Continuous and n times differentiable wavelets are known [2].

The two equivalences in (3.8) are valid for finite-energy deterministic functions in $\mathbb{L}^2(\mathbb{R})$; they also make sense for finite-power deterministic function in $\mathbb{L}^2(I)$, compact $I \subset \mathbb{R}$, and for finite-energy and finite-power random processes w.p.1 on compact $I \subset \mathbb{R}$ when compact scaling function $\phi(t)$ and compact wavelet function $\psi(t)$ are employed [7], [12].

3.3 Wavelet Conditions and Generations

It is clear that one needs to obtain the wavelet filter sequences \underline{h} and \underline{g} in order to perform the DWT. For the computation of the CWT in (2.1), however, one needs to know the wavelet function $\psi(t)$ explicitly. For compactly supported wavelets, knowing \underline{h} and \underline{g} can produce the time-functions $\phi(t)$ and $\psi(t)$. In this section, we discuss the conditions for generating an orthonormal scaling/wavelet pair, and give details for how to produce the time functions. This section is important for the fact that it provides working knowledge for both the DWT and the CWT.

3.3.1 Wavelet conditions

Consider the nested sequence of closed subspaces $\{V_m; m \in \mathbb{Z}\}$ as discussed in section 3.1. The scaling function (at level m) $\phi_m(t)$ is in V_m , which in turn is a proper subset of the closed space V_{m+1} . The basis of V_{m+1} is given by $\{\phi_{m+1,n}(t); n \in \mathbb{Z}\} = \{2^{(m+1)/2}\phi(2^{m+1}t - n); n \in \mathbb{Z}\}$, where we have set $T = 1$ WLOG. Since $\phi_m(t)$ is also in V_{m+1} , we can represent it in terms of the basis functions of V_{m+1} :

$$\phi_m(t) = \sum_n \langle \phi_m(t), \phi_{m+1,n}(t) \rangle \phi_{m+1,n}(t) \quad (3.10)$$

where the inner product $\langle \phi_m(t), \phi_{m+1,n}(t) \rangle$ is given by

$$\begin{aligned}
\langle \phi_m(t), \phi_{m+1,n}(t) \rangle &= \int \phi_m(t) \phi_{m+1,n}^*(t) dt \\
&= \int 2^{m/2} \phi(2^m t) 2^{(m+1)/2} \phi^*(2^{m+1} t - n) dt \\
&= \sqrt{2} \int \phi(t) \phi(2t-n) dt
\end{aligned} \tag{3.11}$$

for real *basic* scaling function $\phi(t)$. Equation (3.11) describes exactly how two consecutive subspaces $V_m \subset V_{m+1}$ are correlated. Note that (3.11) depends only on the scaling function $\phi(t)$, but not on the individual levels m and $m+1$; it holds for any value of m . By defining $h(n)$ via the following *dilation* equation:

$$h(n) = \int \phi(t) \phi(2t-n) dt \tag{3.12}$$

for all n , we can rewrite (3.10) as

$$\phi_m(t) = \sqrt{2} \sum_n h(n) \phi_{m+1,n}(t) \tag{3.13}$$

The dilation equation of (3.12) is the most fundamental equation in wavelet theory. One can proceed along this line of argument and derive the DWT of Figure 3.3. For a scaling function $\phi(t)$ that has a finite support, the number of solutions to (3.12) is finite, and so h is of finite length.

It can be shown that [16]:

$$\int \phi(t) dt = \text{constant} \tag{3.14}$$

and WLOG we can take the constant to be 1. This implies that $\Phi(f) = 1$ at $f = 0$, which means that the scaling function is an impulse response of a lowpass type filter. Integrating both sides of (3.13) with respect to (w.r.t.) time t and letting $m = 0$ yields:

$$1 = \sqrt{2} \sum_n h(n) \int 2^{1/2} \phi(2t-n) dt$$

$$= \sum_n h(n) \quad (3.15)$$

Equation (3.15) is the first wavelet condition, which is a consequence of the nested nature of the increasing subspace sequence $\{V_m\}$. For orthonormal scaling function $\phi(t)$, $\{\phi(t-nT); n \in \mathbb{Z}\}$ is an orthonormal basis for V_0 , and therefore,

$$\begin{aligned} \delta(n) &= \langle \phi(t), \phi(t-n) \rangle \\ &= \langle 2 \sum_k h(k) \phi(2t-k), 2 \sum_j h(j-2n) \phi(2t-j) \rangle \\ &= 4 \sum_k \sum_j h(k) h(j-2n) \frac{1}{2} \delta(k-j) \\ &= 2 \sum_k h(k) h(k-2n) \end{aligned} \quad (3.16)$$

Equation (3.16) is the second wavelet condition; it must hold if the scaling/wavelet system is orthonormal. Performing a discrete Fourier transform on both sides of (3.16) yields the *conjugate filter* equation of (3.5). Note that as a corollary to (3.16), we get by setting $n = 0$ that

$$\frac{1}{2} = \sum_k h^2(k) \quad (3.17)$$

One needs only to find \mathbf{h} such that it satisfies the two wavelet conditions of (3.15) and (3.16). Once \mathbf{h} is known, the sequence \mathbf{g} is given by $g(n) = (-1)^{1-n} h(1-n)$. These two filter sequences are all that are required to perform the DWT.

3.3.2 Generation of wavelet function

In the previous section, we have shown that if the scaling function $\phi(t)$ is known, then we can determine \mathbf{h} and \mathbf{g} and perform the DWT with ease. Conversely, if \mathbf{h} is found by solving the two wavelet conditions, then we can generate $\phi(t)$ and $\psi(t)$ recursively. The construction is as follows. Using (3.13) with $m = 0$, we get the *fundamental recursive equation* for the scaling function $\phi(t)$:

$$\phi(t) = 2 \sum_n h(n) \phi(2t-n) \quad (3.18)$$

Assuming that $\underline{h} = [h(0), h(1), h(2), h(3), \dots, h(M-1)]$, i.e., the \underline{h} sequence has finite length, so that $\phi(t)$ has a compact support on $[0, M-1]$, i.e., $\phi(t)$ is non-zero on this compact interval. We first find the values of $\phi(t)$ on the integers; this is done by using (3.18) to set up the following matrix equation:

$$\begin{bmatrix} \phi(0) \\ \phi(1) \\ \phi(2) \\ \vdots \\ \vdots \\ \vdots \\ \vdots \\ \vdots \\ \vdots \\ \phi(M-1) \end{bmatrix} = 2 \begin{bmatrix} h(0) & 0 & 0 & 0 & 0 & \cdot & \cdot & 0 & 0 & 0 \\ h(2) & h(1) & h(0) & 0 & 0 & \cdot & \cdot & 0 & 0 & 0 \\ h(4) & h(3) & h(2) & h(1) & h(0) & \cdot & \cdot & 0 & 0 & 0 \\ \cdot & h(5) & h(4) & h(3) & h(2) & \cdot & \cdot & 0 & 0 & 0 \\ \cdot & \cdot & \cdot & h(5) & h(4) & \cdot & \cdot & h(1) & h(0) & 0 \\ \cdot & h(3) & h(2) & h(1) \\ h(M-2) & \cdot & \cdot & \cdot & \cdot & \cdot & \cdot & h(5) & h(4) & h(3) \\ 0 & h(M-1) & h(M-2) & \cdot & \cdot & \cdot & \cdot & \cdot & \cdot & h(5) \\ 0 & 0 & 0 & h(M-1) & h(M-2) & \cdot & \cdot & \cdot & \cdot & \cdot \\ 0 & 0 & 0 & 0 & 0 & \cdot & \cdot & \cdot & \cdot & \cdot \\ 0 & 0 & 0 & 0 & 0 & \cdot & \cdot & \cdot & \cdot & \cdot \\ 0 & 0 & 0 & 0 & 0 & \cdot & \cdot & h(M-1) & h(M-2) & \cdot \\ 0 & 0 & 0 & 0 & 0 & \cdot & \cdot & 0 & 0 & h(M-1) \end{bmatrix} \begin{bmatrix} \phi(0) \\ \phi(1) \\ \phi(2) \\ \vdots \\ \vdots \\ \vdots \\ \vdots \\ \vdots \\ \vdots \\ \phi(M-1) \end{bmatrix}$$

(3.19a)

for even M , and

$$\begin{bmatrix} \phi(0) \\ \phi(1) \\ \phi(2) \\ \vdots \\ \phi(M-1) \end{bmatrix} = 2 \begin{bmatrix} h(0) & 0 & 0 & 0 & 0 & 0 & \cdot & 0 & 0 & 0 \\ h(2) & h(1) & h(0) & 0 & 0 & 0 & \cdot & 0 & 0 & 0 \\ h(4) & h(3) & h(2) & h(1) & h(0) & 0 & \cdot & 0 & 0 & 0 \\ \cdot & h(5) & h(4) & h(3) & h(2) & h(1) & \cdot & 0 & 0 & 0 \\ \cdot & \cdot & \cdot & h(5) & h(4) & h(3) & \cdot & h(0) & 0 & 0 \\ \cdot & h(2) & h(1) & h(0) \\ h(M-1)h(M-2) & \cdot & \cdot & \cdot & \cdot & \cdot & \cdot & h(4) & h(3) & h(2) \\ 0 & 0 & h(M-1) & h(M-2) & \cdot & \cdot & \cdot & \cdot & \cdot & h(4) \\ 0 & 0 & 0 & 0 & h(M-1) & h(M-2) & \cdot & \cdot & \cdot & \cdot \\ 0 & 0 & 0 & 0 & 0 & \cdot & \cdot & \cdot & \cdot & \cdot \\ 0 & 0 & 0 & 0 & 0 & \cdot & \cdot & h(M-1) & h(M-2) & \cdot \\ 0 & 0 & 0 & 0 & 0 & \cdot & \cdot & 0 & 0 & h(M-1) \end{bmatrix} \begin{bmatrix} \phi(0) \\ \phi(1) \\ \phi(2) \\ \vdots \\ \phi(M-1) \end{bmatrix} \quad (3.19b)$$

for odd M . In general, solving (3.19a) or (3.19b) is equivalent to finding the eigenvector corresponding to the eigenvalue $\lambda = 1$ of the matrix A given in below:

$$\Phi = A \Phi \quad (3.20)$$

We may impose the additional condition on Φ that $\sum_n \phi(n) = 1$. When the matrix A has zero determinant there can be multiple $\lambda = 1$ solutions to (3.20). Once we know the values of $\phi(t)$ on the integers, we can compute its values on the $\frac{1}{2}$ -integers by using the fundamental recursion of (3.18) as follows:

$$\phi\left(\frac{k}{2}\right) = 2 \sum_n h(n) \phi(k-n) \quad (3.21)$$

and so-forth for on the $\frac{1}{4}, \frac{1}{8}, \frac{1}{16}, \frac{1}{32}, \dots$ -integers, recursively. Thus, the scaling function $\phi(t)$, which has support on the compact time interval $[0, M-1]$, can be determined explicitly for t being a dyadic number. Since the dyadic numbers (i.e., multiples of 2^{-k} , for all $k \geq 0$) are dense in \mathbb{R} , the function $\phi(t)$ can be determined at all times t in the limit.

The wavelet function $\psi(t)$ is similarly computed as follows. Since $\psi(t) \in W_0 \subset V_1$, we can represent $\psi(t)$ as a linear combination of the basis functions of V_1 :

$$\begin{aligned}\psi(t) &= \sum_n \langle \psi(t), 2^{1/2} \phi(2t-n) \rangle 2^{1/2} \phi(2t-n) \\ &= 2 \sum_n g(n) \phi(2t-n)\end{aligned}\tag{3.22}$$

which is a recursion similar to (3.18). Since we already know $\phi(t)$ on the dyadic numbers, it follows that $\psi(t)$ can be computed using (3.22). The filter sequence g is a flip-alternate-negation of h , and we can set $g = [g(0), g(1), g(2), \dots, g(M-1)]$ so that $\psi(t)$ also has a compact support on the time interval $[0, M-1]$.

At this point we have shown how to generate $\psi(t)$ for the CWT. The question is: How do we find $h(n)$ in the first place? Although one may guess or even trial and error to find a h sequence that satisfy the two wavelet conditions, in reality it is a difficult task to find a scaling/wavelet pair that has nice analytical properties. Nonetheless, several researchers have succeeded in systematically generating wavelet functions. We show some of their work in the following.

3.3.3 Compactly supported wavelets examples

First of all, the simplest compactly supported wavelet is the Haar wavelet. It has a compact support on $[0, 1]$, with $h = [1/2, 1/2]$ and $g = [1/2, -1/2]$. The Haar scaling/wavelet pair is shown in Figure 3.4.a. Note that the functions are not continuous.

Daubechies [2] has proposed a class of compactly supported orthonormal wavelets and she gave the h s for $M = 4, 6, 8, 10, 12, 14, 16, 18, 20$. For example, the Daubechies 4-coefficient wavelet has $h = [h(0), h(1), h(2), h(3)]$ given by:

$$\begin{aligned}h(0) &= \frac{1+\sqrt{3}}{8}, & h(1) &= \frac{3+\sqrt{3}}{8} \\ h(2) &= \frac{3-\sqrt{3}}{8}, & h(3) &= \frac{1-\sqrt{3}}{8}\end{aligned}\tag{3.23}$$

Note that $h(0)+h(1)+h(2)+h(3) = 1$, and $h^2(0)+h^2(1)+h^2(2)+h^2(3) = 1/2$. Substituting \underline{h} into (3.19) we find the eigenvector for $\lambda = 1$ to be

$$[\phi(0), \phi(1), \phi(2), \phi(3)] = [0, 1.366, -0.366, 0] \quad (3.24)$$

The corresponding scaling function $\phi(t)$ and the wavelet function $\psi(t)$ (D_4) are recursively computed, using (3.18) and (3.22), respectively, and they are plotted in Figure 3.4.b We also show the Daubechies 10-coefficient scaling/wavelet (D_{10}) pair in Figure 3.4.c and the 20-coefficient scaling/wavelet (D_{20}) pair in Figure 3.4.d Observe that D_{20} looks like a modulated Gaussian. Also note that the Daubechies wavelets are increasingly smoother in time and better-contained in the frequency spectrum.

Pollen [19] has shown that it is possible to parametrize compactly supported wavelets. In particular, for $M = 6$, using a pinched torus, he was able to give a parametrization of the \underline{h} sequence as follows:

$$\begin{aligned} h(0) &= [(1 + \cos \alpha + \sin \alpha)(1 - \cos \beta - \sin \beta) + 2 \sin \beta \cos \alpha] / 8 \\ h(1) &= [(1 - \cos \alpha + \sin \alpha)(1 + \cos \beta - \sin \beta) - 2 \sin \beta \cos \alpha] / 8 \\ h(2) &= [1 + \cos(\alpha - \beta) + \sin(\alpha - \beta)] / 4 \\ h(3) &= [1 + \cos(\alpha - \beta) - \sin(\alpha - \beta)] / 4 \\ h(4) &= [1 - h(0) - h(2)] / 2 \\ h(5) &= [1 - h(1) - h(3)] / 2 \end{aligned} \quad (3.25)$$

where $-\pi \leq \alpha, \beta < \pi$ are the two parametrizing angles. It is indeed a very nice and important result. As an example, the Haar wavelet has parametrization $\alpha = \beta$, for any α . As another example, we randomly generate $\alpha = 0.2172$ and $\beta = 0.3359$ and use (3.25) to obtain

$$\underline{h} = [0.0055, -0.0322, 0.4686, 0.5278, 0.0259, 0.0044]. \quad (3.26)$$

It turns out that this is a valid wavelet sequence; we carry out the recursive generation and we plot the resulting scaling function and wavelet function in Figure 3.4.e. This wavelet has dual passbands. Note that the scaling function and the wavelet function are orthonormal basis functions. One can experiment with (3.26) to generate very crazy looking wavelet functions.

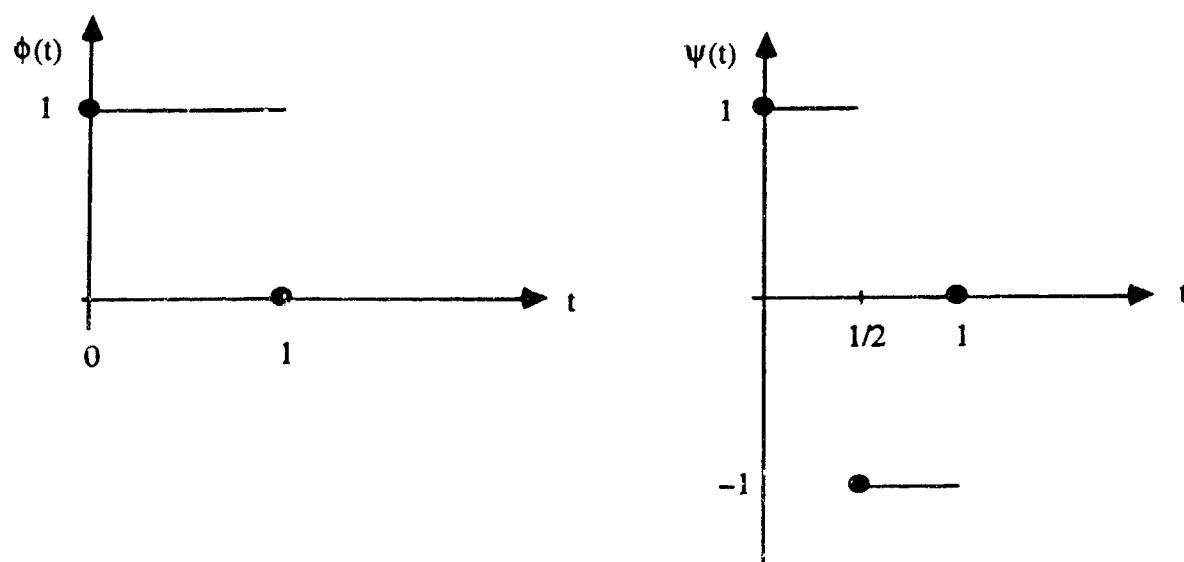


Figure 3.4.a The Haar scaling function and wavelet function.

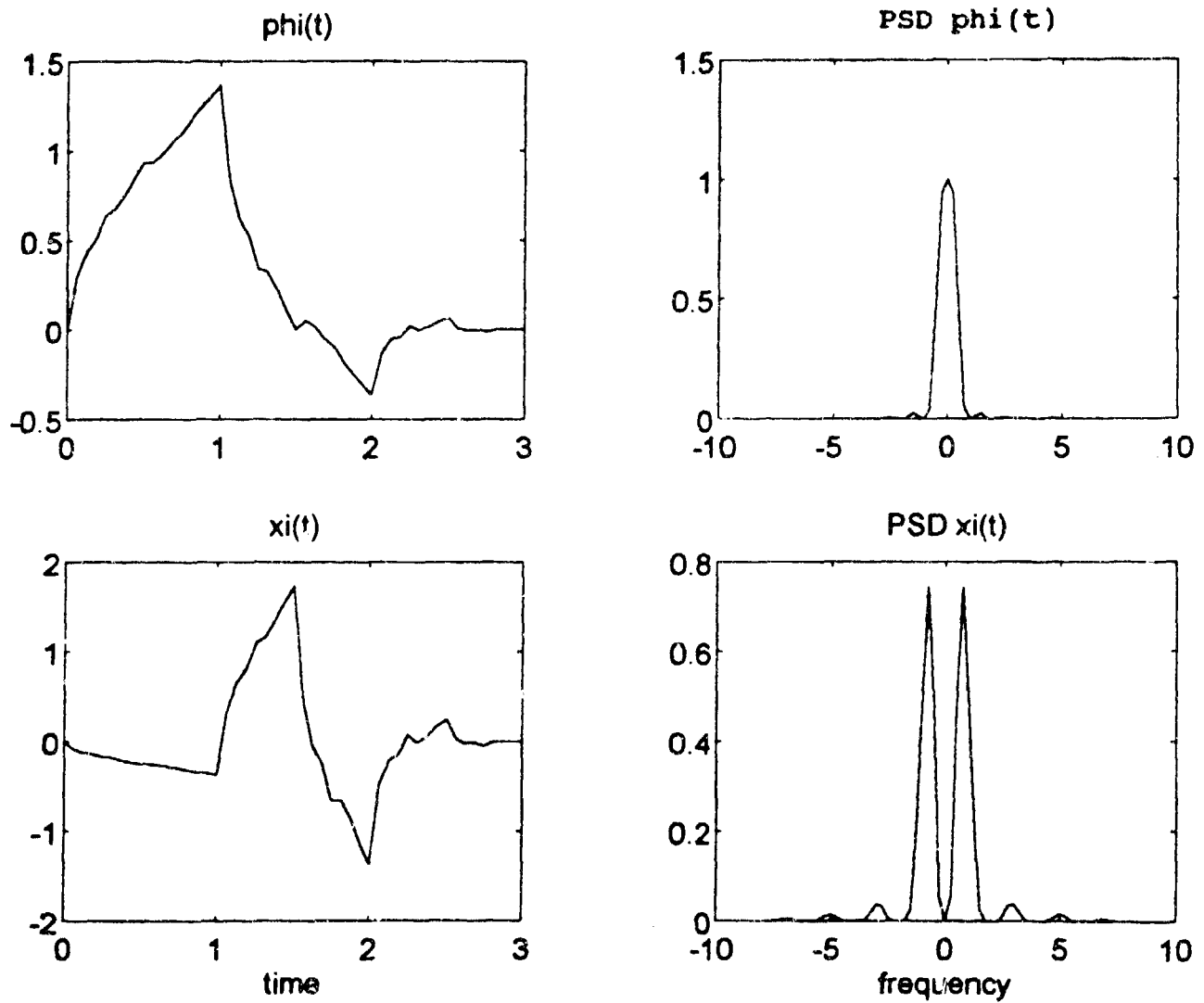


Figure 3.4.b Daubechies 4-coefficient (D_4) scaling function and wavelet function, and their energy spectra.

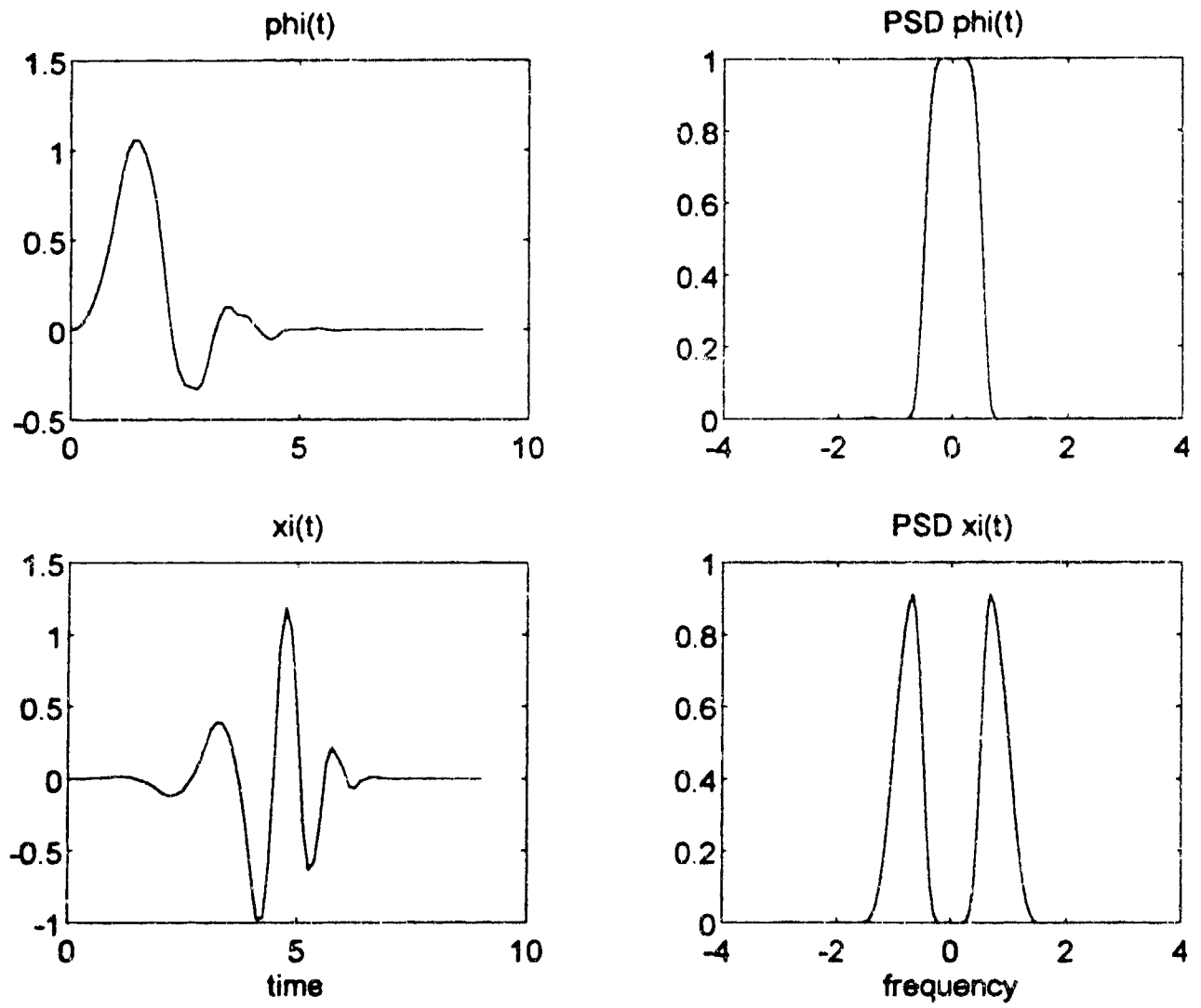


Figure 3.4.c Daubechies 10-coefficient (D_{10}) scaling function and wavelet function, and their energy spectra.

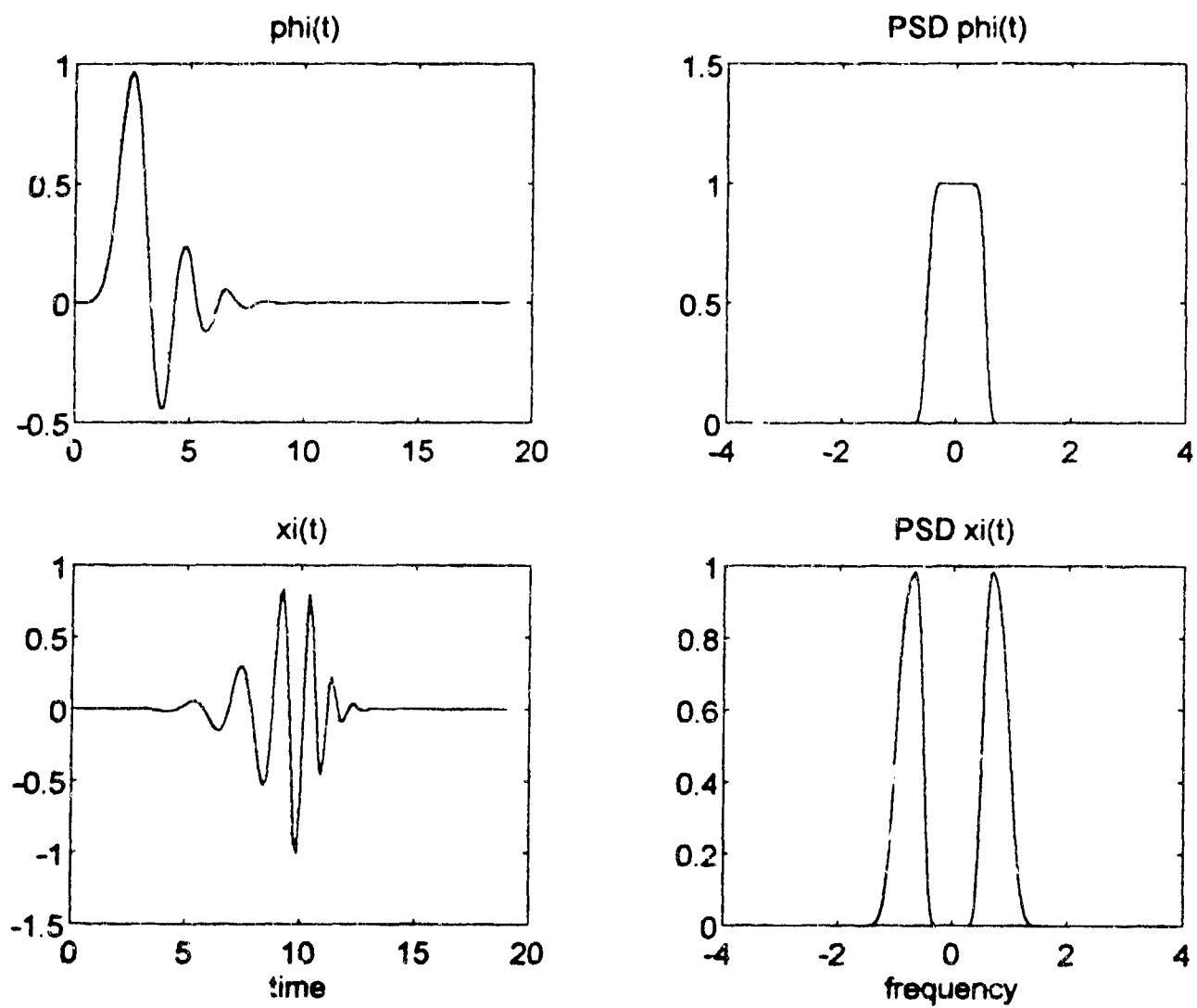


Figure 3.4.d Daubechies 20-coefficient (D_{20}) scaling function and wavelet function, and their energy spectra.

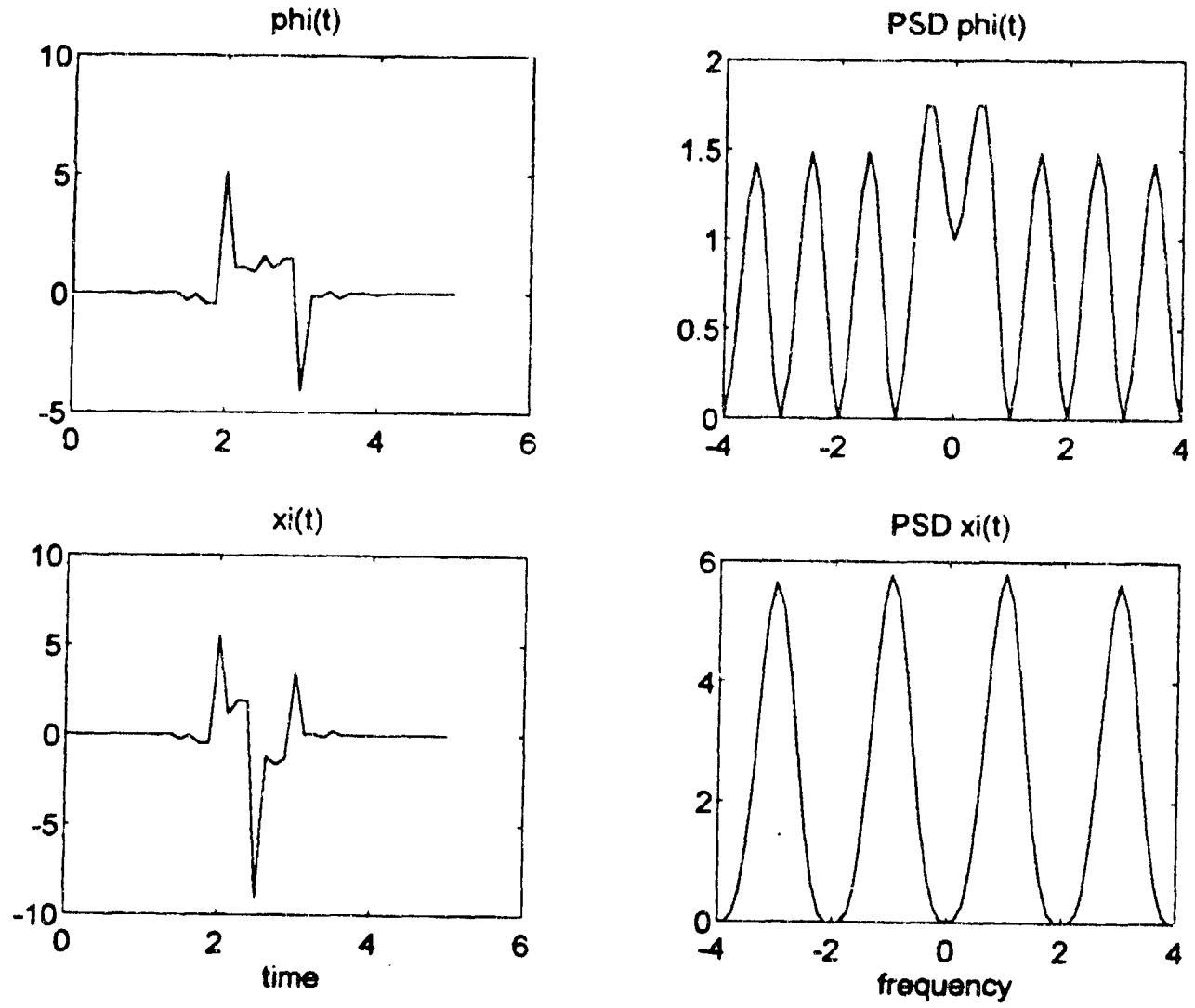


Figure 3.4.e A 6-coefficient scaling function and wavelet function with Pollen parametrization $\alpha = 0.2172$, $\beta = 0.3359$, and their energy spectra.

3.4 Multiple-Phase Discrete Wavelet Transform

In digital signal analysis, what one has at hand is a sequence of N samples, $x(nT)$, where T is the sampling period and $n = 0, 1, 2, \dots, N_s-1$. It is convenient to consider an auxiliary function $x_0(t)$ in V_0 : $x_0(t) = \sum_n b_{0,n} \phi_{0,n}(t)$ by setting $b_{0,n} = x(nT)$ at resolution level 0, which is the highest level available. Using a recursive filtering algorithm, the so-called discrete wavelet transform (DWT) of section 3.2, one can compute the lower-level resolution coefficients as (Fig. 3.3):

$$\begin{aligned} b_{m-1}(i) &= \sum_k \sqrt{2} h(k) b_m(2i + k) \\ d_{m-1}(i) &= \sum_k \sqrt{2} g(k) b_m(2i + k) \end{aligned} \quad (3.27)$$

for $m = 0, -1, -2, -3, \dots$. Here, $\underline{h} = [h(-M+2), h(-M+3), \dots, h(0), h(1)]$ and $\underline{g} = [g(-M+2), g(-M+3), \dots, g(0), g(1)]$ are the appropriate conjugate-quadrature discrete-time filter responses.

The h coefficients are obtained by the dilation equation $h(k) = \int_{-\infty}^{\infty} \phi(t) \phi(2t - k) dt$. We have set $g(k) = (-1)^{-M+3-k} h(-M+3-k)$ so that the time indexes for the b 's and d 's are always non-negative. We also assumed that both ϕ and ψ have compact supports so that \underline{h} and \underline{g} have only finite number of filter taps ($= M$). Roughly speaking, the approximation coefficients $b_{m,n}$ capture the approximate information in the signal sequence at resolution level m , while the difference coefficients $d_{m,n}$ retain the detail information going from resolution level $m-1$ to m . The DWT has important applications in signal analysis, particularly in compression, detection, and classification. The choice of ϕ and ψ (hence \underline{h} and \underline{g}) is such that the signal is localized as much as possible in both time and frequency. Unfortunately, the DWT is not time invariant. If the signal sequence is time-shifted by one unit to become $\underline{b} = [0, b_{0,0}, b_{0,1}, b_{0,2}, \dots, b_{0,N-1}]$ then the corresponding DWT is not time-shifted and it will be completely different from the old DWT. This will not present a problem to the reconstruction of the signal sequence; however, the merits of DWT for signal detection and classification may be diminished.

We note that for dyadic DWT, there are two different sets of DWT at each level; we name them as "phase-0" and "phase-1" decompositions. Referring to Fig. 3.5, for phase-0 decomposition, the 0-th coefficient at resolution level $m-1$ is $[\underline{h}(1)] \cdot [\underline{b}_{m,0}]$, the 1-st coefficient is $[\underline{h}(-1), \underline{h}(0), \underline{h}(1)] \cdot [\underline{b}_{m,0}, \underline{b}_{m,1}, \underline{b}_{m,2}]$ where " \cdot " denotes dot-product, the 2-nd coefficient is

$[h(2), h(-1), h(0), h(1)] \cdot [b_{m,1}, b_{m,2}, b_{m,3}, b_{m,4}]$, and so forth. On the other hand, the phase-1 coefficients will read as $[h(0), h(1)] \cdot [b_{m,0}, b_{m,1}]$, $[h(-2), h(-1), h(0), h(1)] \cdot [b_{m,0}, b_{m,1}, b_{m,2}, b_{m,3}]$, $[h(-2), h(-1), h(0), h(1)] \cdot [b_{m,2}, b_{m,3}, b_{m,4}, b_{m,5}]$,

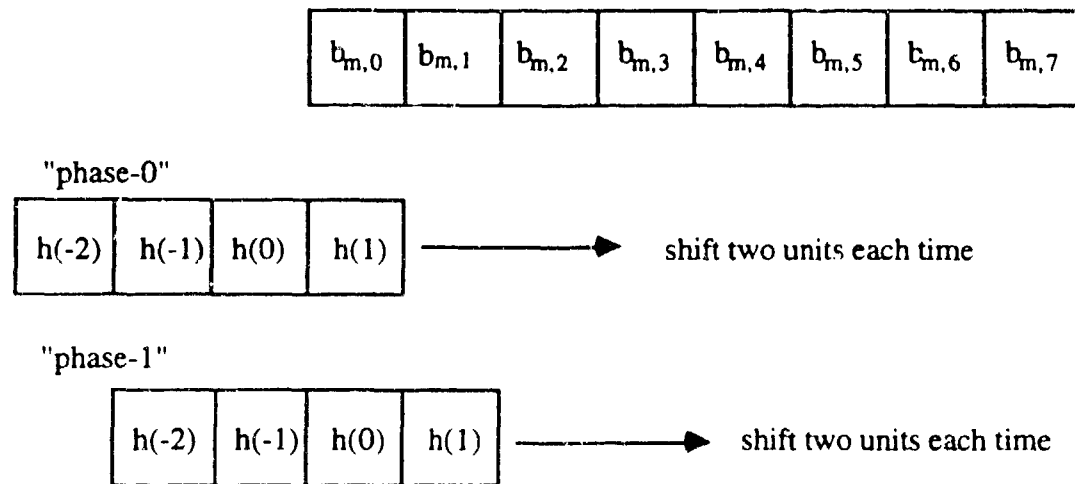


Figure 3.5 Two phases of wavelet decomposition.

We have proposed a multiple-phase DWT (MP/DWT) for signal analysis [10], [14], [13]. The key to this MP/DWT is to construct new filter sequences h_m and g_m ($m \leq -1$) at each decomposition level by inserting $2^{-(m+1)} - 1$ number of zeros between every two subsequent filter coefficients.

The MP approximation coefficients at level $m - 1$, time indexed i , is given by the dot product of h_m and b'_m , where b'_m is the MP approximation coefficient sequence at level m denoted by $b'_m =$

$(b'_{m,0}, b'_{m,1}, b'_{m,2}, \dots)$. Specifically, we have

$$b'_{m-1,i} = \sum_{k=-M+2-(M-1)(2^{-m}-1)}^1 \sqrt{2} h_m(k) b'_{m,i+k-1}$$

and

$$d'_{m-1,i} = \sum_{k=-M+2-(M-1)(2^{-m}-1)}^1 \sqrt{2} g_m(k) b'_{m,i+k-1} \quad (3.28)$$

The manner that the phase-0 and phase-1 coefficients are interleaved at each level may be described by the tree diagram shown in Fig. 3.6. For a k -level decomposition, there are altogether 2^k

possible phases of decomposition. Each path in the tree of Fig. 3.6 represents an unique phase-sequence. One may choose to decompose the signal along any one of these 2^k phase-sequences and obtain a different DWT. Interleaving all of them yields our MP/DWT. Note that knowing the phase-sequence, one can trace back in the tree and reconstruct the signal from the DWT. Note that MP/DWT is a redundant transformation. It may be regarded as a discrete approximation of the continuous wavelet transform for $x_0(t)$. Its time-invariant property may be useful for some signal detection problems. The MP/DWT can be used to detect PSK signals, but we shall report the results elsewhere. For data compression applications, one can maximize the data compression ratio by optimizing over the 2^k phase-sequences.

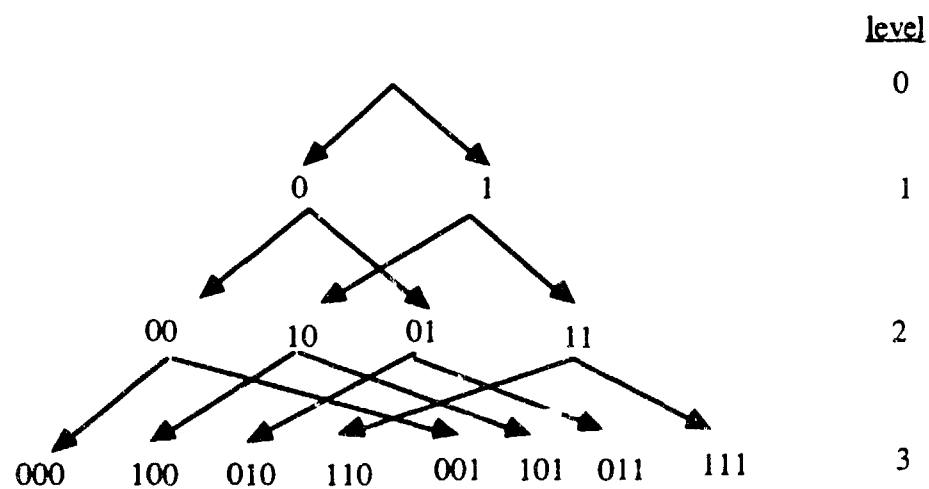


Figure 3.6 Different phases of wavelet decomposition.

4. DETECTION OF PSK SIGNALS

We now use the CWT of (2.1) to analyze PSK signals. Viewing the CWT in a time-scale plane, we attempt to identify qualitative and quantitative features that would reveal the exact occasions of the phase shifts. First, we consider a baseband rectangular wave and its noisy versions. Next, we analyze a 180° phase shift in a sinusoid and its noisy versions. Haar, Daubechies, and complex modulated Gaussian wavelets will be employed in the decompositions.

4.1 Rectangular Wave

4.1.1 Haar wavelet

A baseband rectangular wave and its CWTs using the Haar wavelet are shown in Figure 4.1.a. The rectangular wave signal has a normalized duration of 1 second. The signal sequence $x(nT)$ has length equal to 65 and it changes sign at $n = 9, 25, 41,$ and 57 , which corresponds to $t = nT = 9/64, 25/64, 41/64$ and $57/64$ seconds, respectively. The Haar wavelet $\psi(t) = \psi_0(t)$ was shown in Figure 4.1.a. The transforms $CW_x(nT, 2^{-m})$ is computed using (2.1) for $n = 0, 1, \dots, 64$, and $m = 0, 1, 2, \dots, 6$; they are shown in sequential order in Figure 4.1.a. Note that there are some end effects due to the finite signal window and we would ignore these end effects. At low level of decomposition, i.e., $m = 0, 1,$ or 2 , the CWT has good frequency resolution and we see that the oscillating frequency of the signal is revealed. At higher level of decomposition, the time resolution is getting better and the CWT reveals the sign change instances with increasing accuracy. Specifically, at $m = 6$, a positive "spike" in the CWT shows a $+1$ to -1 sign change, and a negative "spike" shows a -1 to $+1$ sign change. The Haar wavelet is matched to the sign change so the good time resolution is expected. However, at high time resolution, the wavelet filter has large bandwidth. When there is noise, a lot of noise energy will be collected and the signal CWT will be smeared, as we will show in the next figure.

We add noise to the rectangular wave and show the CWTs in Figure 4.1.b and 4.1.c. Power of the signal sequence is $E(x^2(nT)) = 1$. The random noise sequence is Gaussian with mean zero and variance s^2 . Define the signal-power to noise-power ratio as:

$$\text{SNR} = \frac{\text{signal sequence power}}{\text{noise sequence power}} \quad (4.1)$$

In Figure 4.1.b, the SNR is 10 dB and in Figure 4.1.c the SNR is 5 dB. We see that the low level CWTs are not severely affected so we still have good frequency resolution. At higher level, the CWTs are increasingly smeared by the noise, especially at $m = 6$. This is because the output signal-power to noise-power ratio, SNR_o , defined by:

$$SNR_o = \frac{\text{filtered signal sequence power}}{\text{filtered noise sequence power}} \quad (4.2)$$

is decreasing exponentially with m . Note that the wavelet filter (with impulse response $\psi_m(t)$) has bandwidth $B = 2 \cdot 2^m \sigma_0$ and so the filtered noise power is increasing exponentially with m for wideband noise. The filtered signal power, however, will decrease with m since the r.m.s. center frequency of the wavelet filter is moving towards $f = +\infty$ and smaller and smaller amount of signal energy will be collected. If the signal is a wideband spread-spectrum signal instead of a narrowband signal, then it is possible that SNR_o will remain large for many levels of decompositions. This suggests that WT is suitable for detecting spread-spectrum signals.

For $SNR = 10$ dB as in Figure 4.1.b, one can observe from the CWT at $m = 4$ and $m = 6$ that there are 4 sign changes. However, when one attempts to pinpoint the exact times of occurrence by viewing the CWT at $m = 6$, only the changes at $t = 9/64$ and $41/64$ can be located with confidence.

For $SNR = 5$ dB in Figure 4.1.c, the noise power is too much for the CWT to reveal good time-resolutions. Only the oscillating frequency of the rectangular wave can be revealed. The Haar wavelet does not work well in noise because its poor spectral properties, i.e., its spectrum decays too slow and has too many sidelobes.

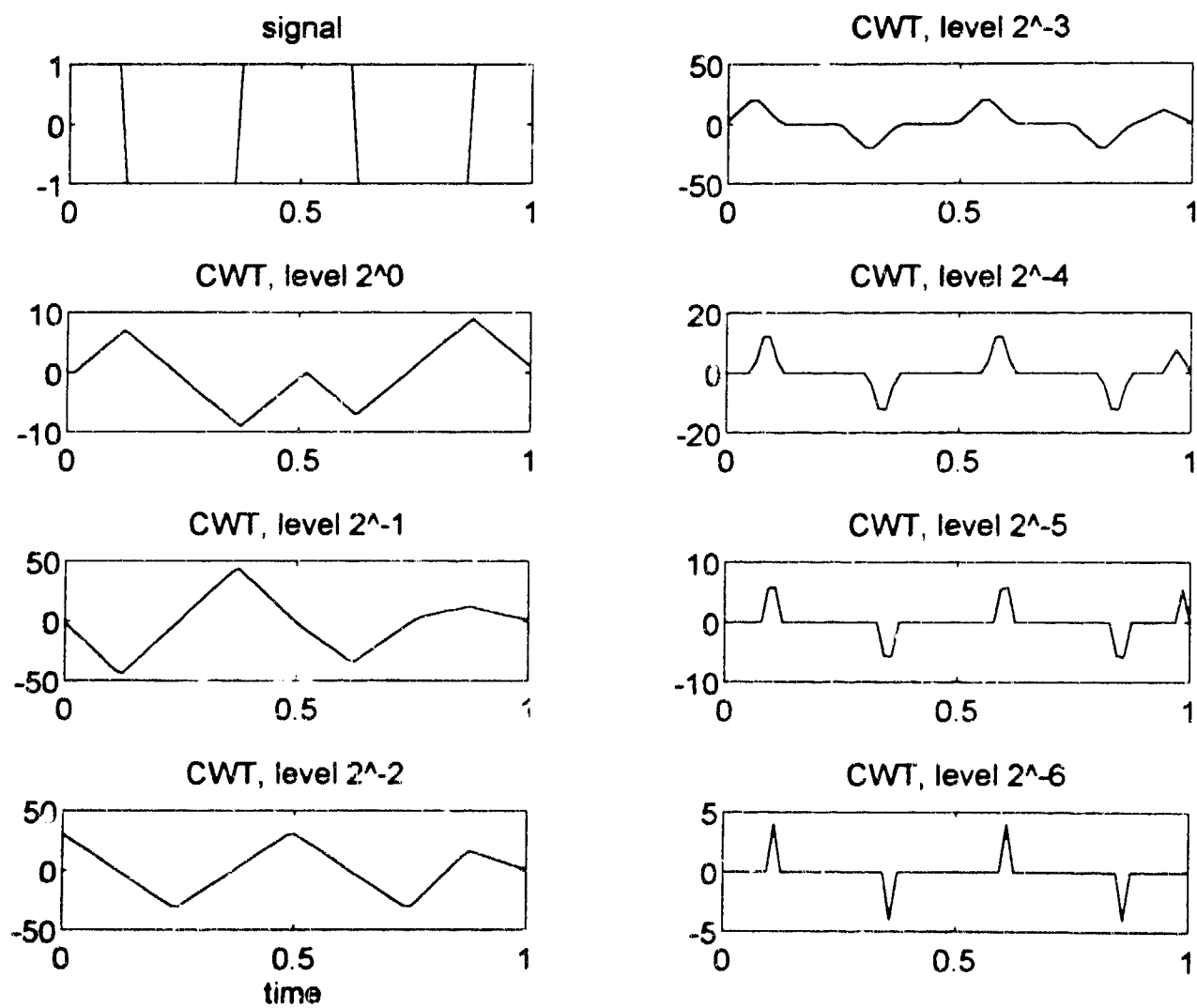


Figure 4.1.a CWT of rectangular wave with Haar wavelet. No noise.

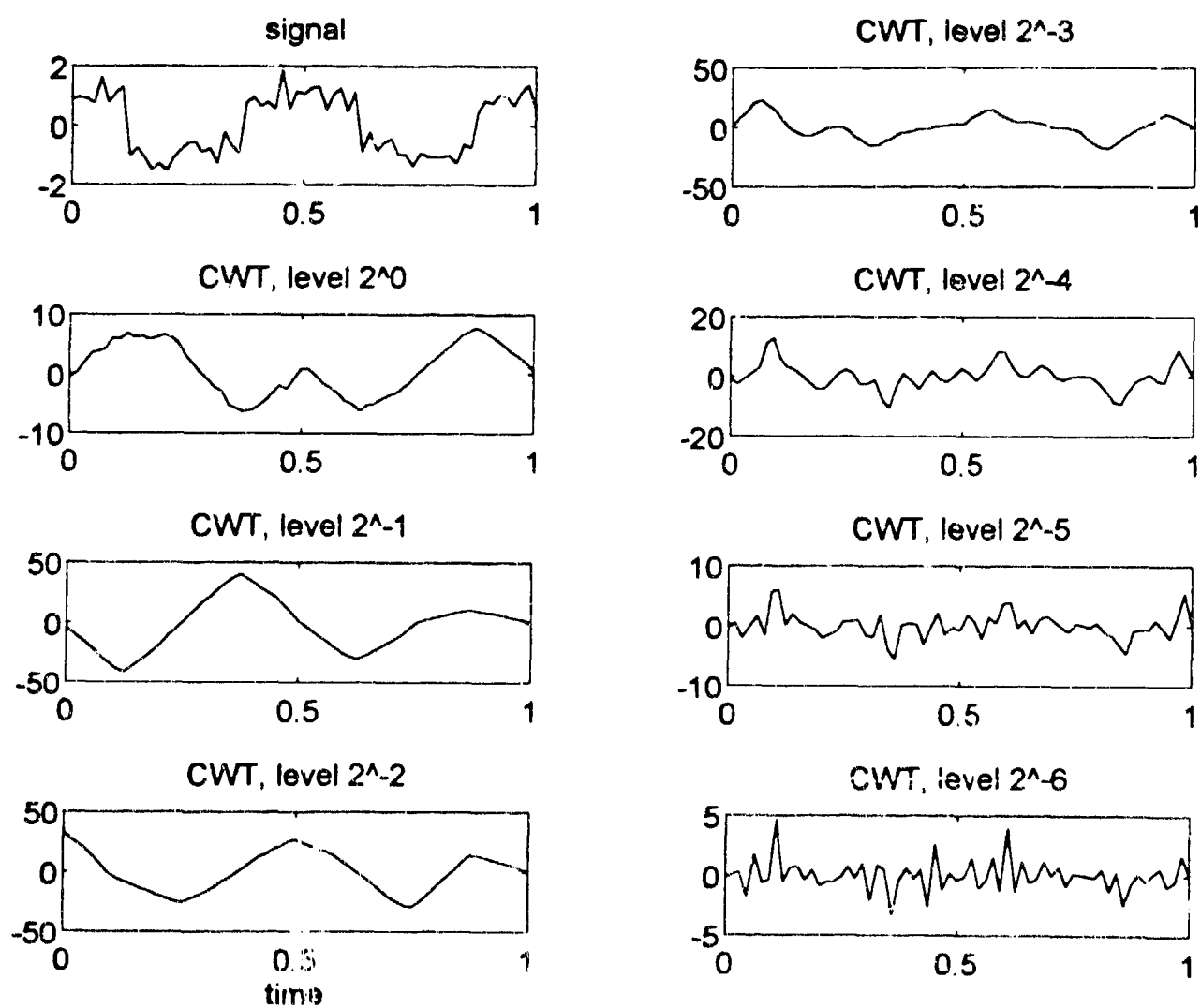


Figure 4.1.b CWT of rectangular wave with Haar wavelet. SNR = 10 dB.

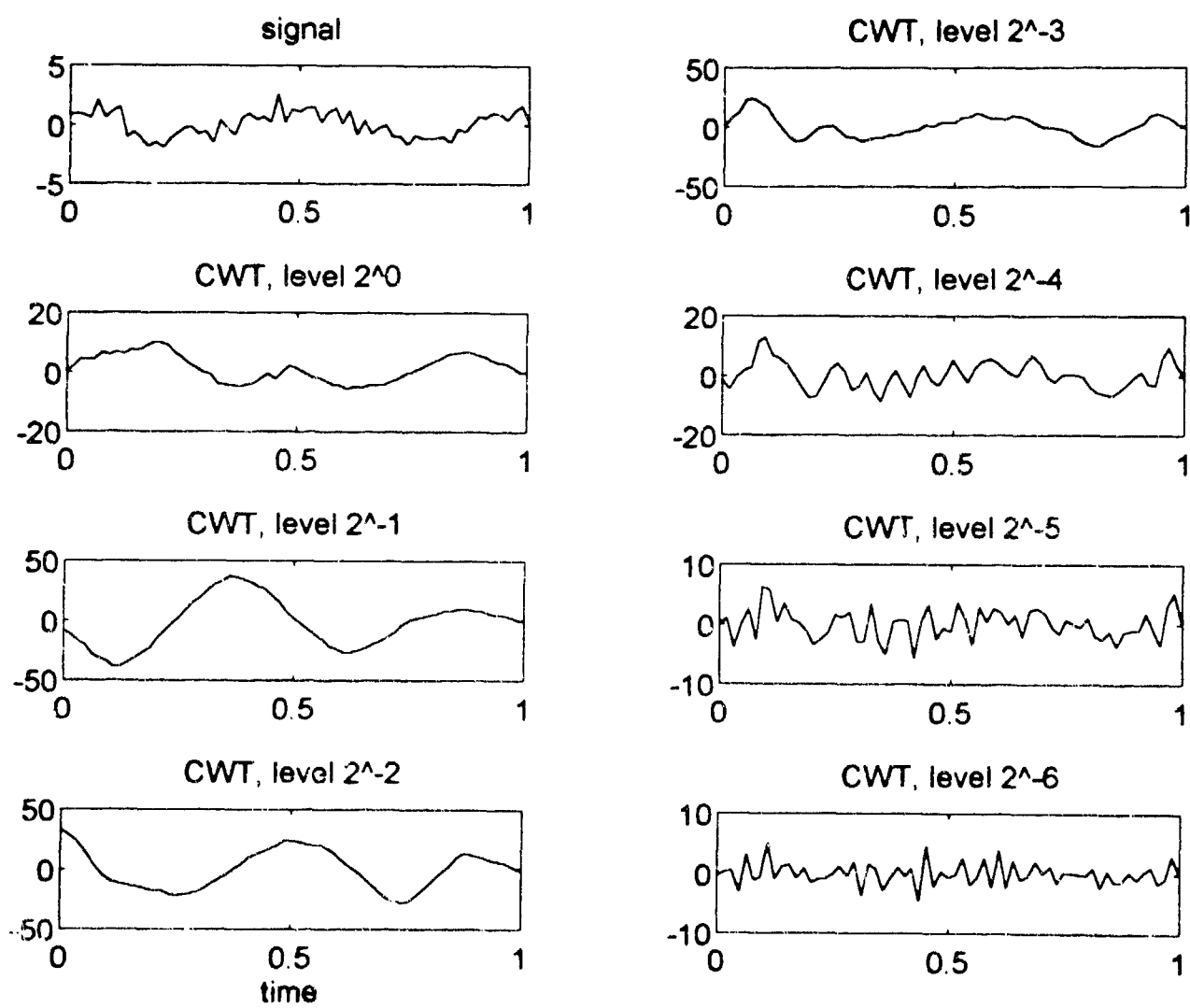


Figure 4.1.c CWT of rectangular wave with Haar wavelet. SNR = 5 dB.

4.1.2 Daubechies wavelet

Daubechies wavelets have better frequency properties than the Haar wavelet. However, they are not matched (in time) to the sign change in the rectangular wave. We show the CWTs for the rectangular wave with Daubechies 10-coefficient wavelet (D_{10}) in Figures 4.2.a, 4.2.b, and 4.2.c for the noiseless, SNR = 10 dB, and SNR = 5 dB cases, respectively. The wavelet is first normalized in time so that it is confined to the interval $[0, 1]$ at level $m = 0$.

When there is no noise, the Daubechies wavelet is also capable in locating the sign changes with high time-resolution as shown in Figure 4.2.a. Furthermore, because its frequency spectrum is more confined than the Haar wavelet, the CWT at low level reveals the oscillating frequency of the rectangular wave with greater resolution.

When SNR = 10 dB, the performance is worse, as shown in Figure 4.2.b. At levels $m = 3$ and $m = 4$, it is possible to identify the first and the third sign changes correctly, just as in the Haar case. But there is a false indication around $t = 0.4$. When SNR = 5dB, this Daubechies wavelet is seen to perform not much better than the Haar wavelet, as shown in Figure 4.2.c.

The problem with both Haar and Daubechies, as well as other unmodulated wavelets is that they are not tunable. It is difficult to select or "customize" the passband center frequency for a specific signal, thereby the wavelet filter may miss most of the signal energy. It is also not possible to have a relatively narrow bandwidth at high frequencies. The complex modulated Gaussian wavelet is capable to alleviate these shortcomings.

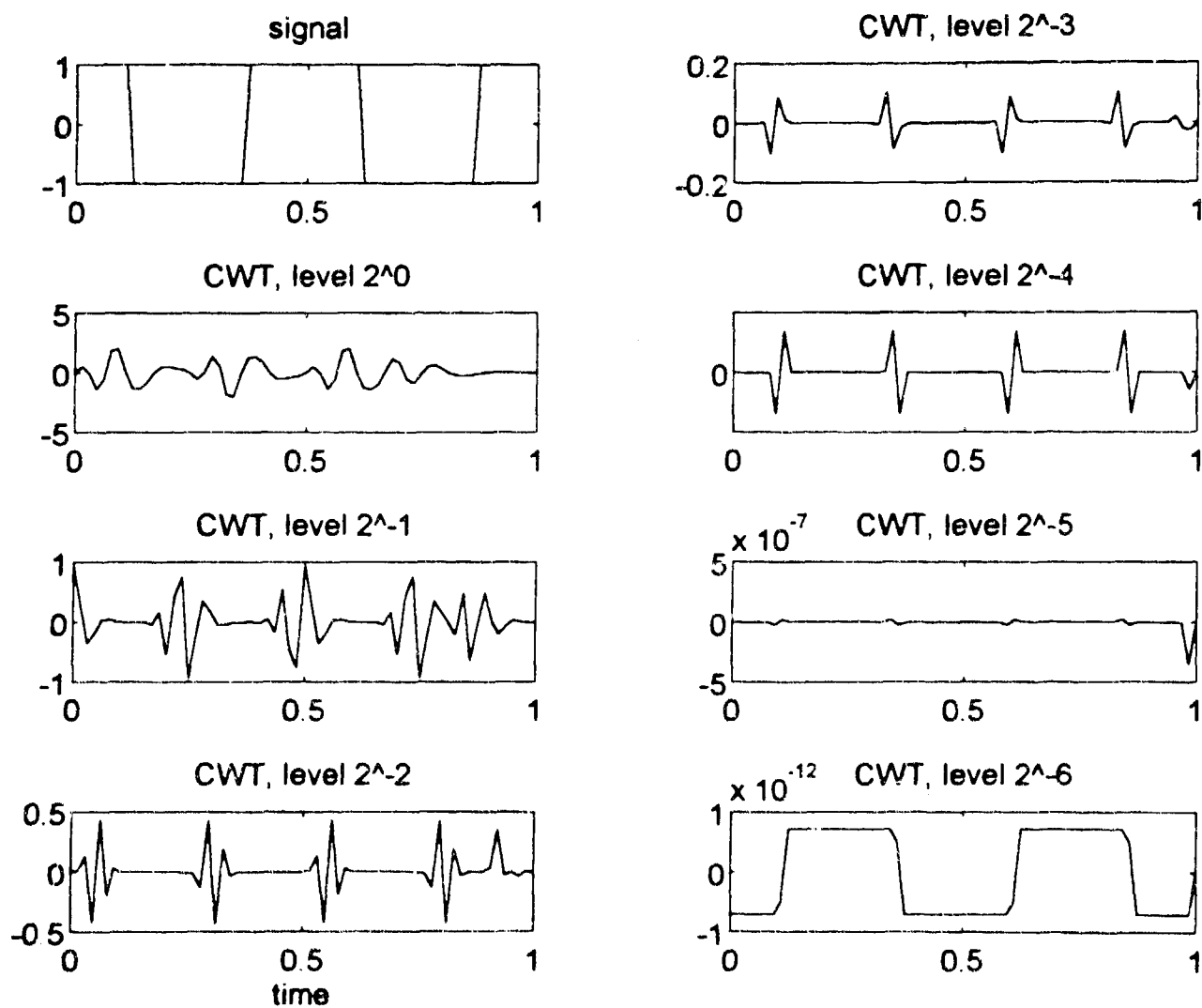


Figure 4.2.a CWT of rectangular wave with Daubechies 10-coefficient wavelet. No noise.

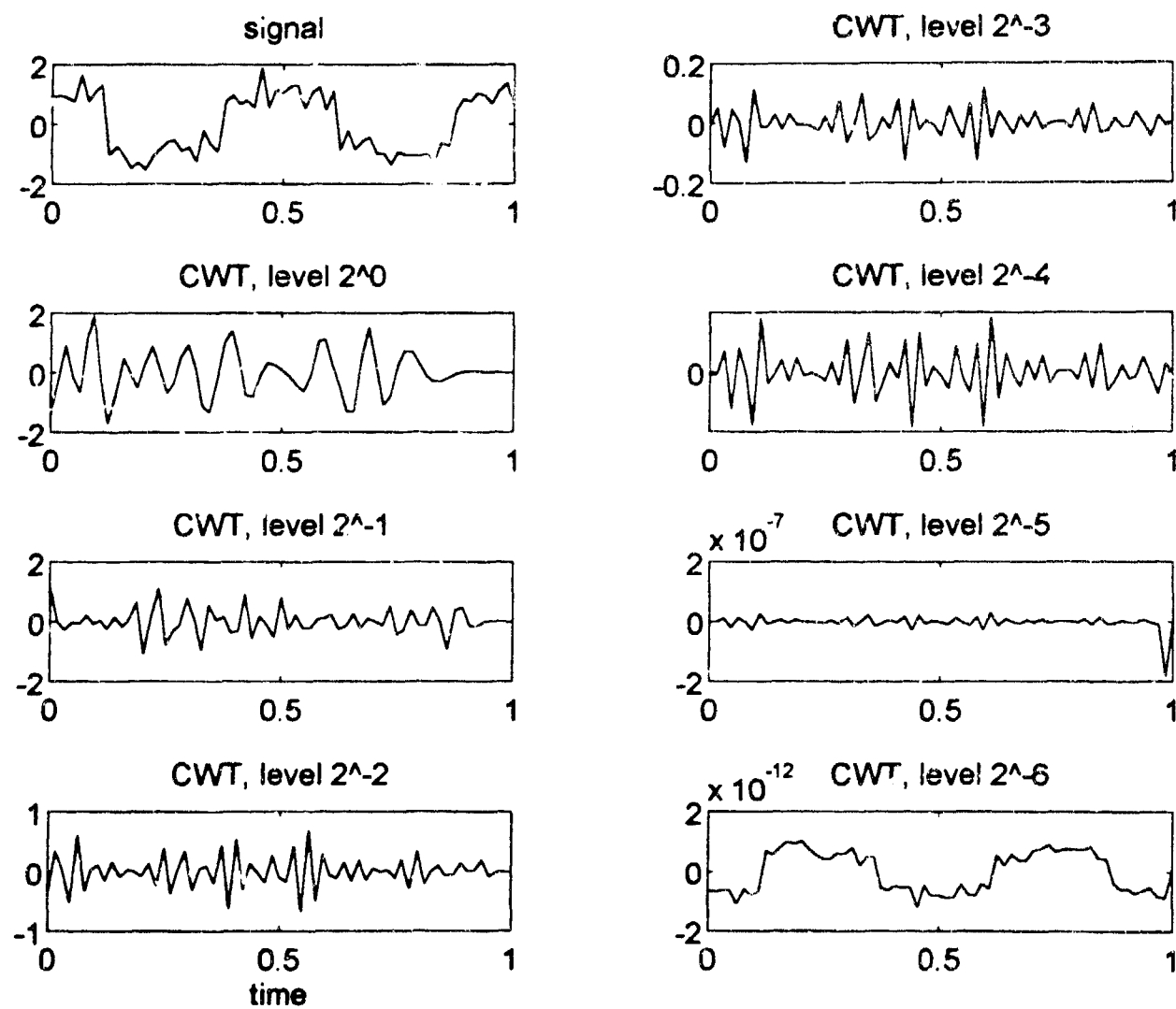


Figure 4.2.b CWT of rectangular wave with Daubechies 10-coefficient wavelet.
SNR = 10 dB.

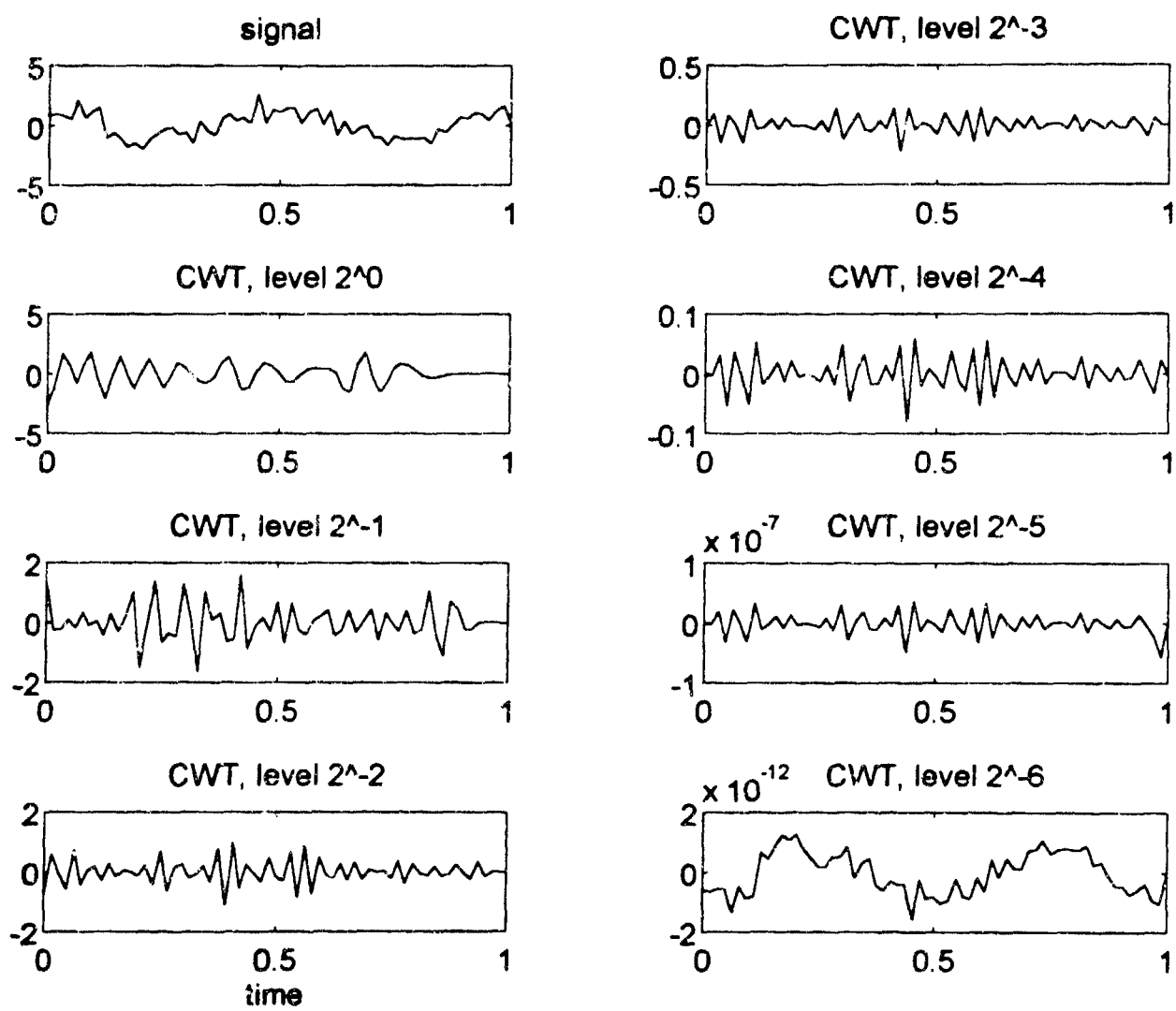


Figure 4.2.c CWT of rectangular wave with Daubechies 10-coefficient wavelet.
SNR = 5 dB.

4.1.3 Complex modulated Gaussian wavelet

By changing the modulating frequency, f_ψ , of the complex modulated Gaussian wavelet, one can place the wavelet passband center frequency practically anywhere on the positive frequency axis. Changing f_ψ , as well as σ , in (2.10) gives us two extra dimensions to expose the signal features. Although there may be a lot of redundancy, this approach essentially gives us a tunable, variable-bandwidth multiresolutional analysis of the signal. It is also possible to adapt the analysis to different types of signal and noise.

For simpler presentation, we fix $\sigma = 0.12$ and only vary f_ψ to be 4, 8, and 16 Hz. For the noiseless case, we show the corresponding time-scale decompositions (which are complex valued) in Figures 4.3.a – 4.3.f. The first three figures depict the magnitudes of the CWTs, while the last three figures show the phases of the CWTs. Consider the magnitude plots in Figures 4.3.a, 4.3.b, and 4.3.c. There are altogether $3 \times 7 = 21$ snapshots of the wavelet filtered rectangular wave. Each set of 7 snapshots start with a different center frequency f_ψ and the filter banks scan the frequency axis as m increases from 0 to 6. Most of these 21 magnitude plots do correctly reveal the sign change times (with different time-resolutions) and would be useful in the noisy cases. The phase plots in Figures 4.3.d, 4.3.e, and 4.3.f confirm the sign change times, and in addition they also reveal the polarity (+ to – or – to +) of each change. Note that when there is noise and the magnitude plots are not conclusive, we can consult the phase plots for a confirmation. This alternative source of information is not available in decompositions using real wavelets.

For the case when $\text{SNR} = 10$ dB, we show the magnitude plots for $f_\psi = 4, 8, 16$ in Figures 4.4.a, 4.4.b, and 4.4.c. In Figure 4.4.b at $m = 6$, the magnitude plot of the CWT clearly indicate that there are sign changes at the four correct instance, although in addition there is a possible false indication at $t \approx 0.4$. Figure 4.4.a at $m = 3, 4$, and 5 confirm that the findings are due to the signal but not the noise. Note that in Figure 4.4.c, the magnitude plots are not informative and certainly are not conclusive; the choice of $f_\psi = 16$ is too large for this particular signal.

When $\text{SNR} = 5$ dB, we show one set of magnitude plots of the CWT in Figure 4.5 with $f_\psi = 8$. At level $m = 6$, the CWT reveals correctly the first, second, and the third sign change, probably misses the fourth one and falsely add one at $t \approx 0.4$. The results can then be referenced with other magnitude plots using a different modulating frequency. Comparing with the Haar and the Daubechies wavelets, the performance of the complex modulated Gaussian is better, especially in the noisy cases.

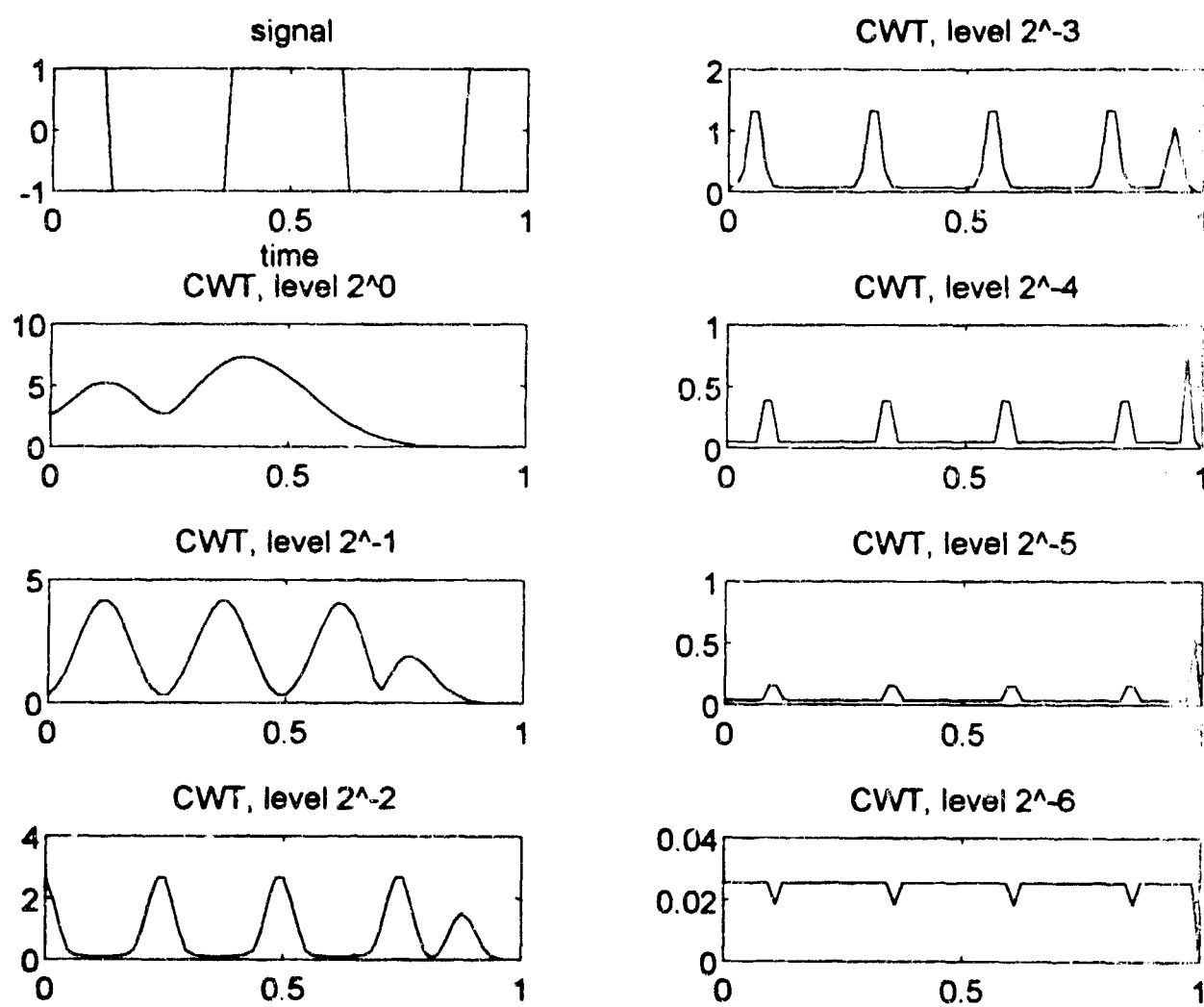


Figure 4.3.a Magnitude of CWT of rectangular wave with complex modulated Gaussian wavelet. $\sigma = 0.12$, $f_{\psi} = 4$. No noise.

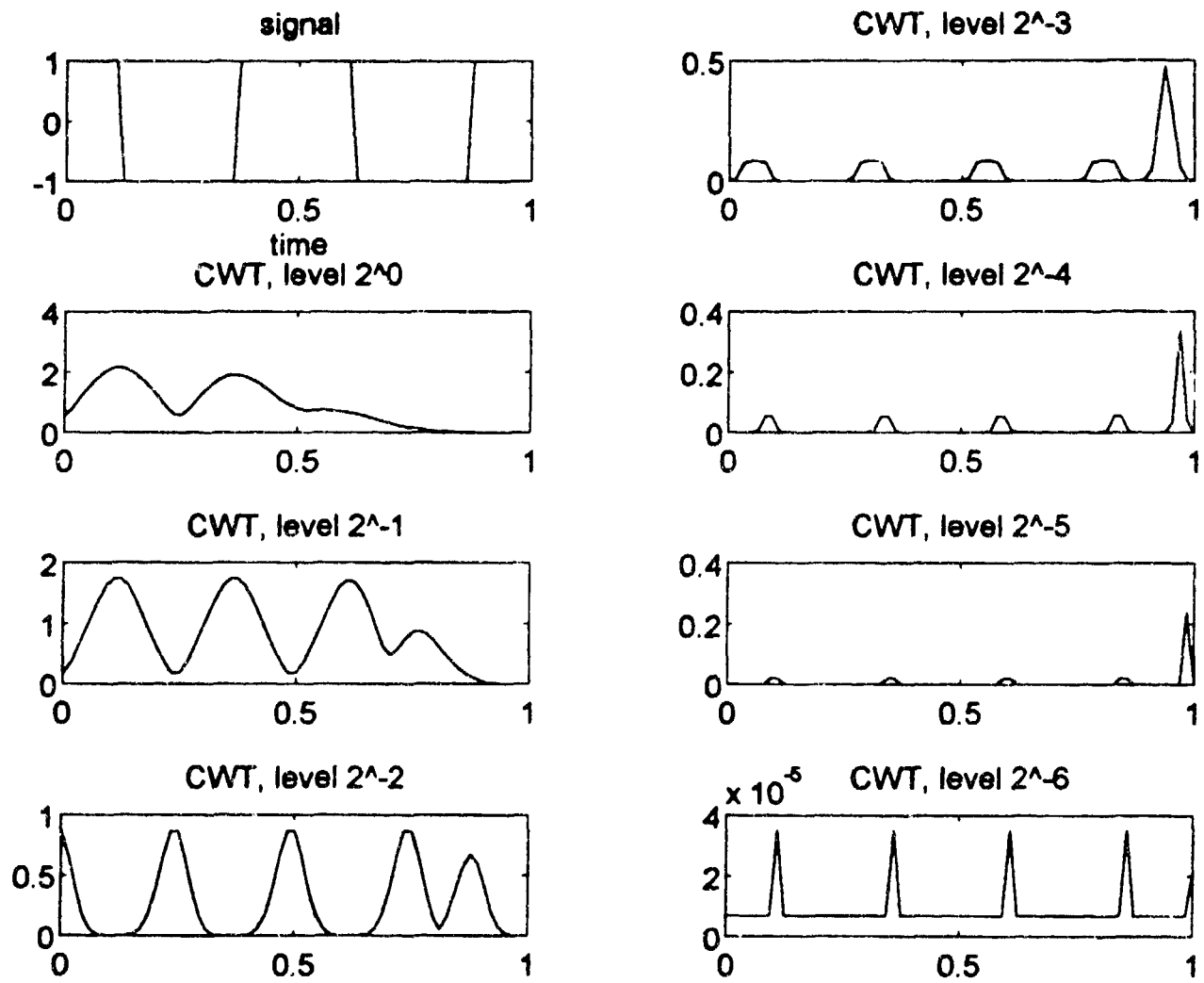


Figure 4.3.b Magnitude of CWT of rectangular wave with complex modulated Gaussian wavelet. $\sigma = 0.12$, $f_{\psi} = 8$. No noise.

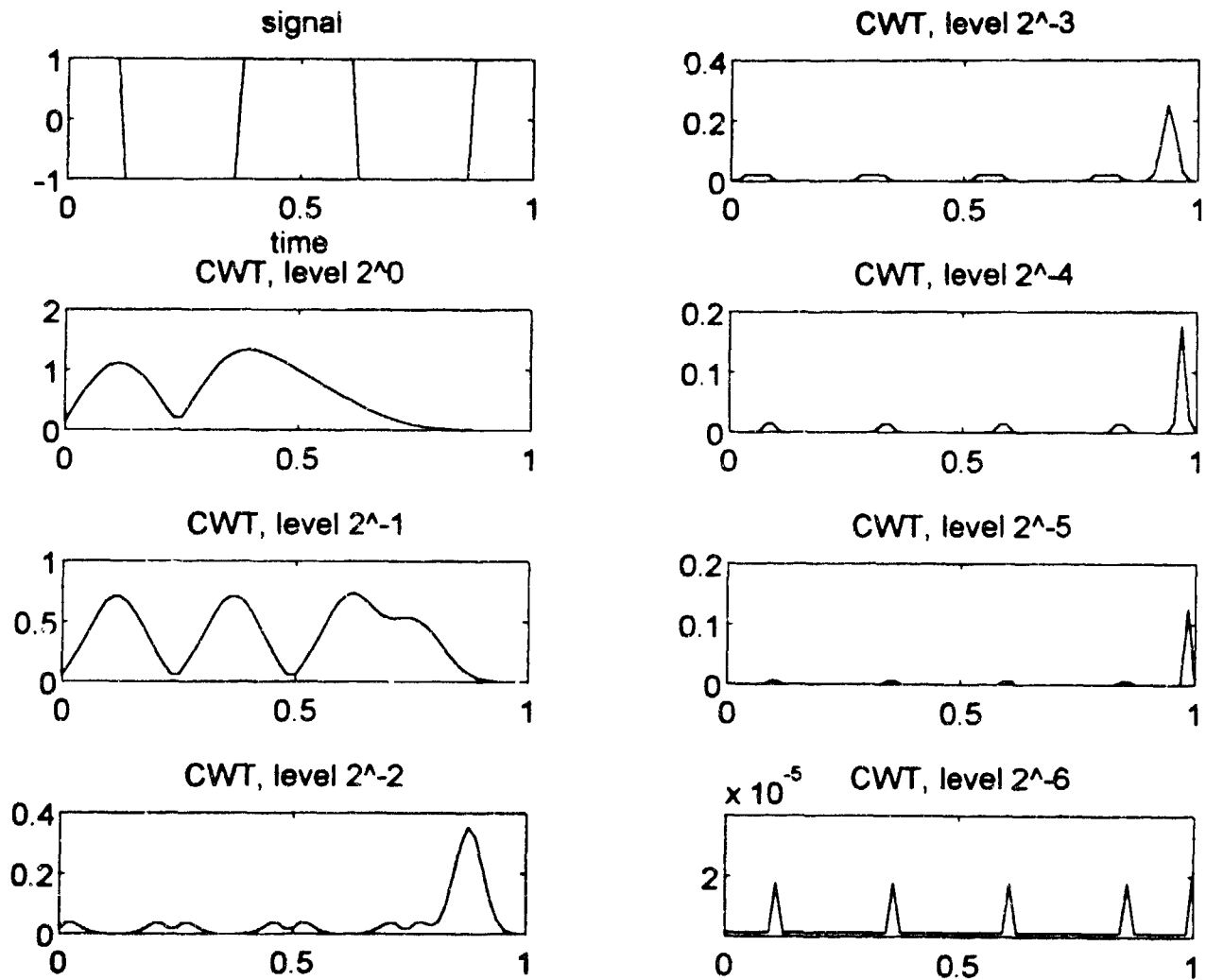


Figure 4.3.c Magnitude of CWT of rectangular wave with complex modulated Gaussian wavelet. $\sigma = 0.12$, $f_{\psi} = 16$. No noise.

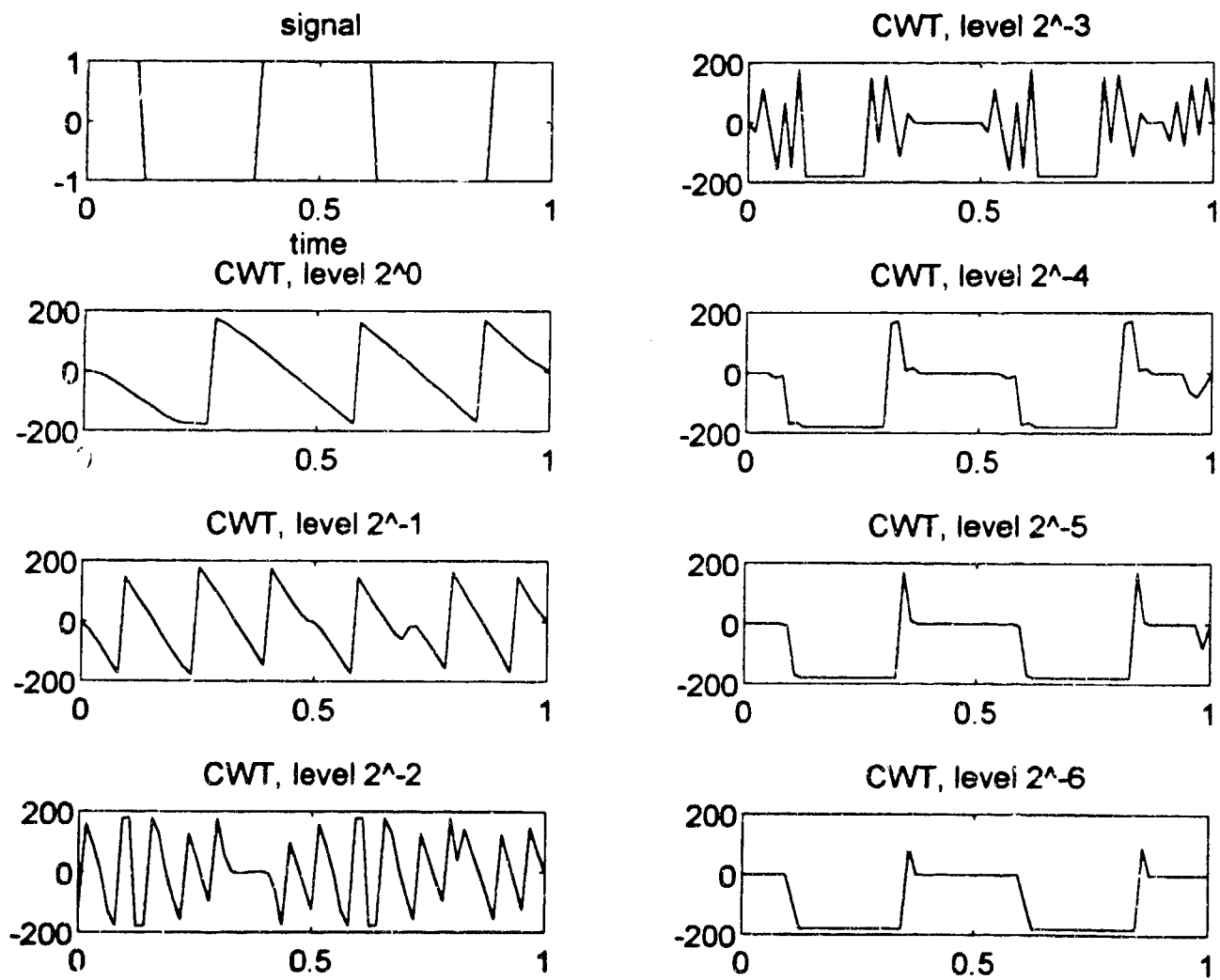


Figure 4.3.d Phase of CWT of rectangular wave with complex modulated Gaussian wavelet. $\sigma = 0.12$, $f_\psi = 4$. No noise.

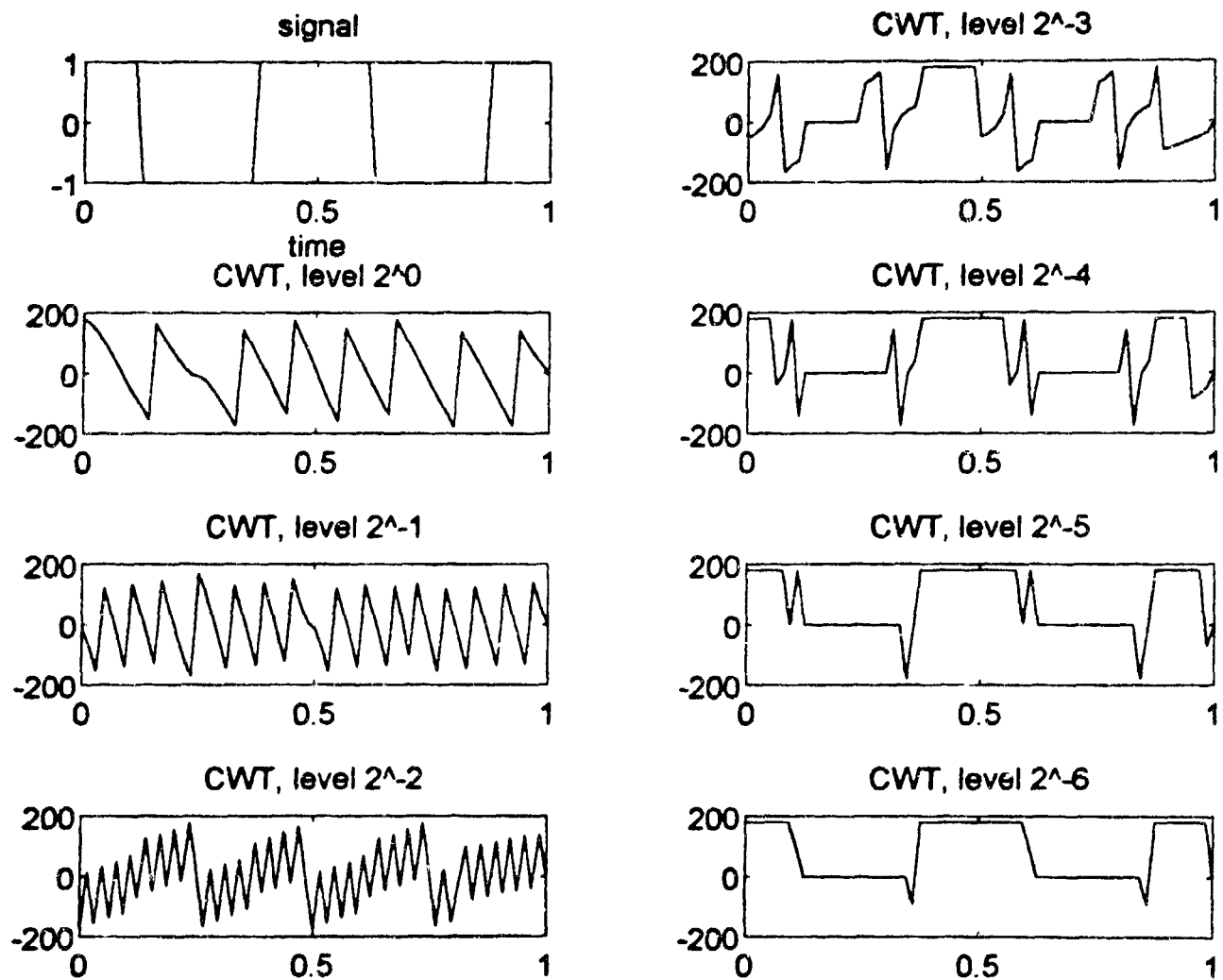


Figure 4.3.e Phase of CWT of rectangular wave with complex modulated Gaussian wavelet. $\sigma = 0.12$, $f_{\psi} = 8$. No noise.

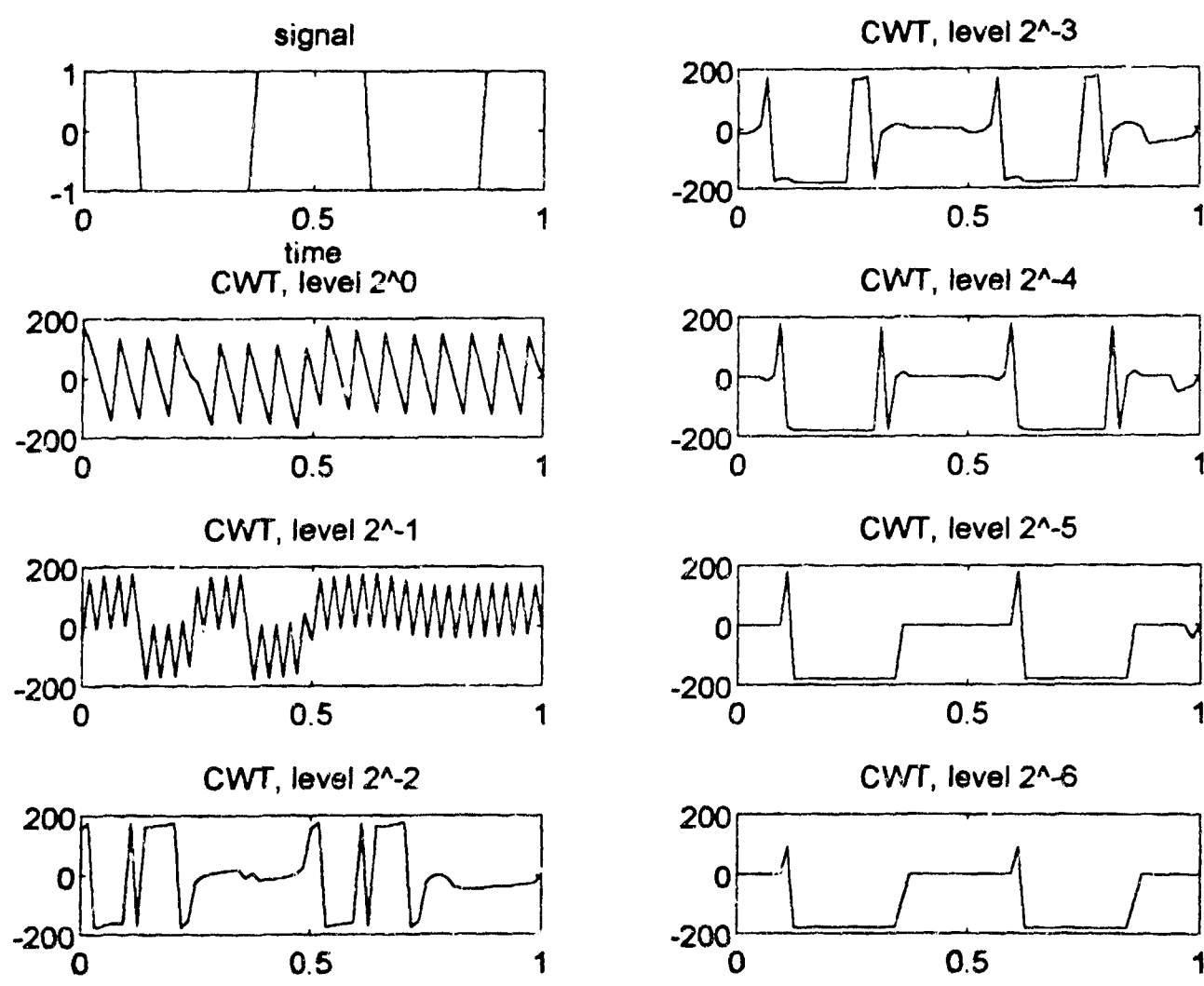


Figure 4.3.f Phase of CWT of rectangular wave with complex modulated Gaussian wavelet. $\sigma = 0.12$, $f_{\psi} = 16$. No noise.

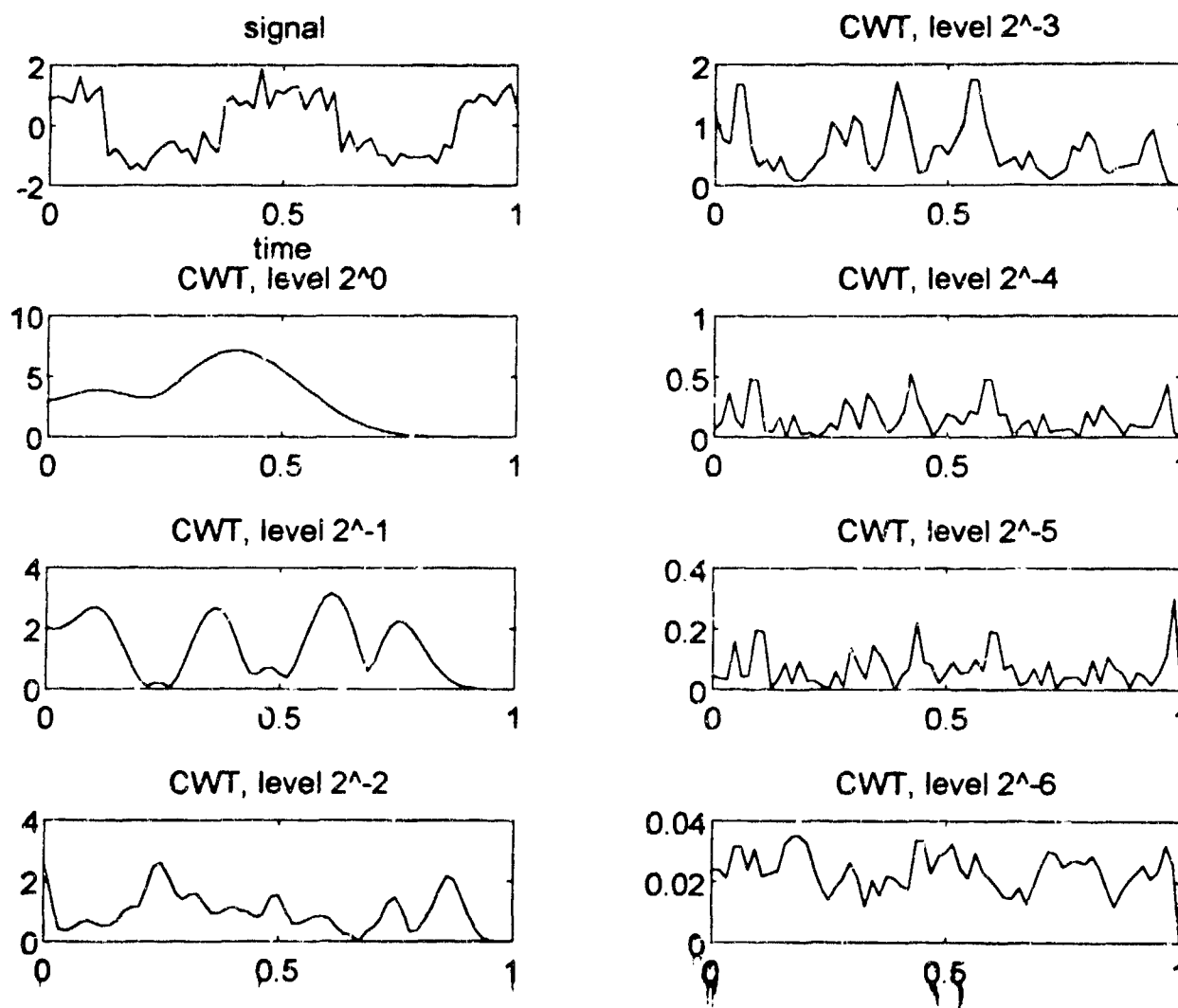


Figure 4.4.a Magnitude of CWT of rectangular wave with complex modulated Gaussian wavelet. $\sigma = 0.12$, $f_{\psi} = 4$. SNR = 10 dB.

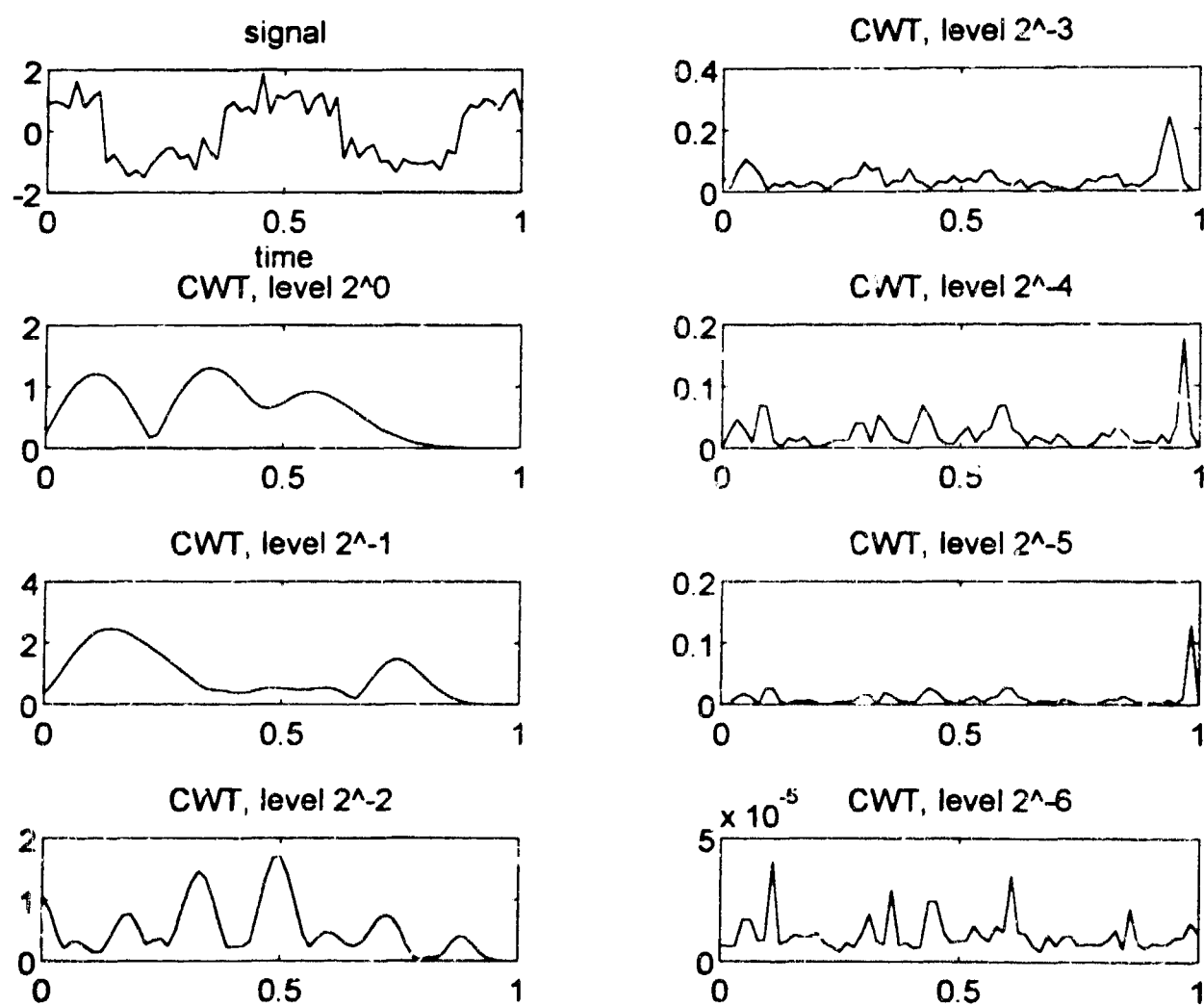


Figure 4.4.b Magnitude of CWT of rectangular wave with complex modulated Gaussian wavelet. $\sigma = 0.12$, $f_{\psi} = 8$. SNR = 10 dB.

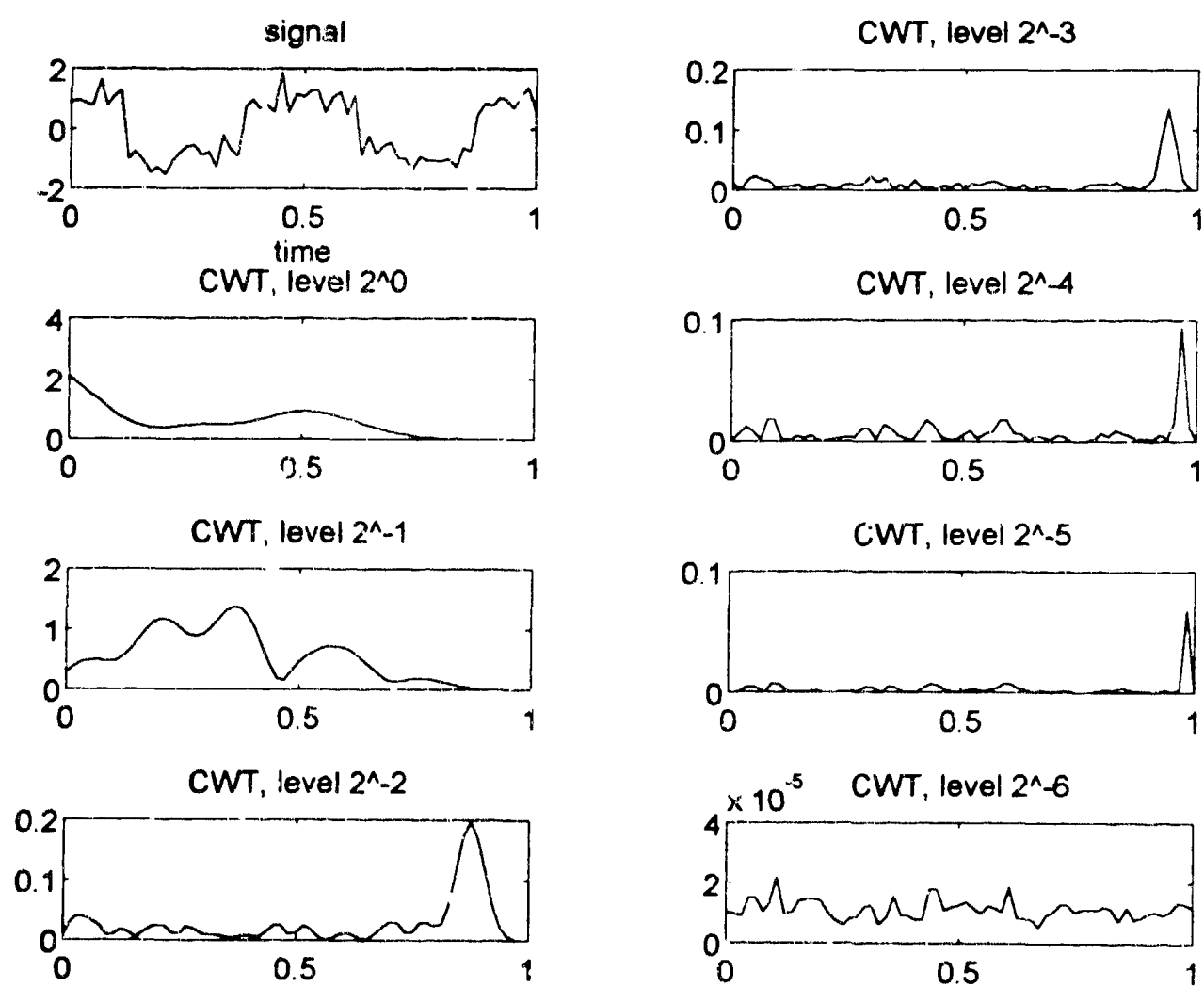


Figure 4.4.c Magnitude of CWT of rectangular wave with complex modulated Gaussian wavelet. $\sigma = 0.12$, $f_{\psi} = 16$. SNR = 10 dB.

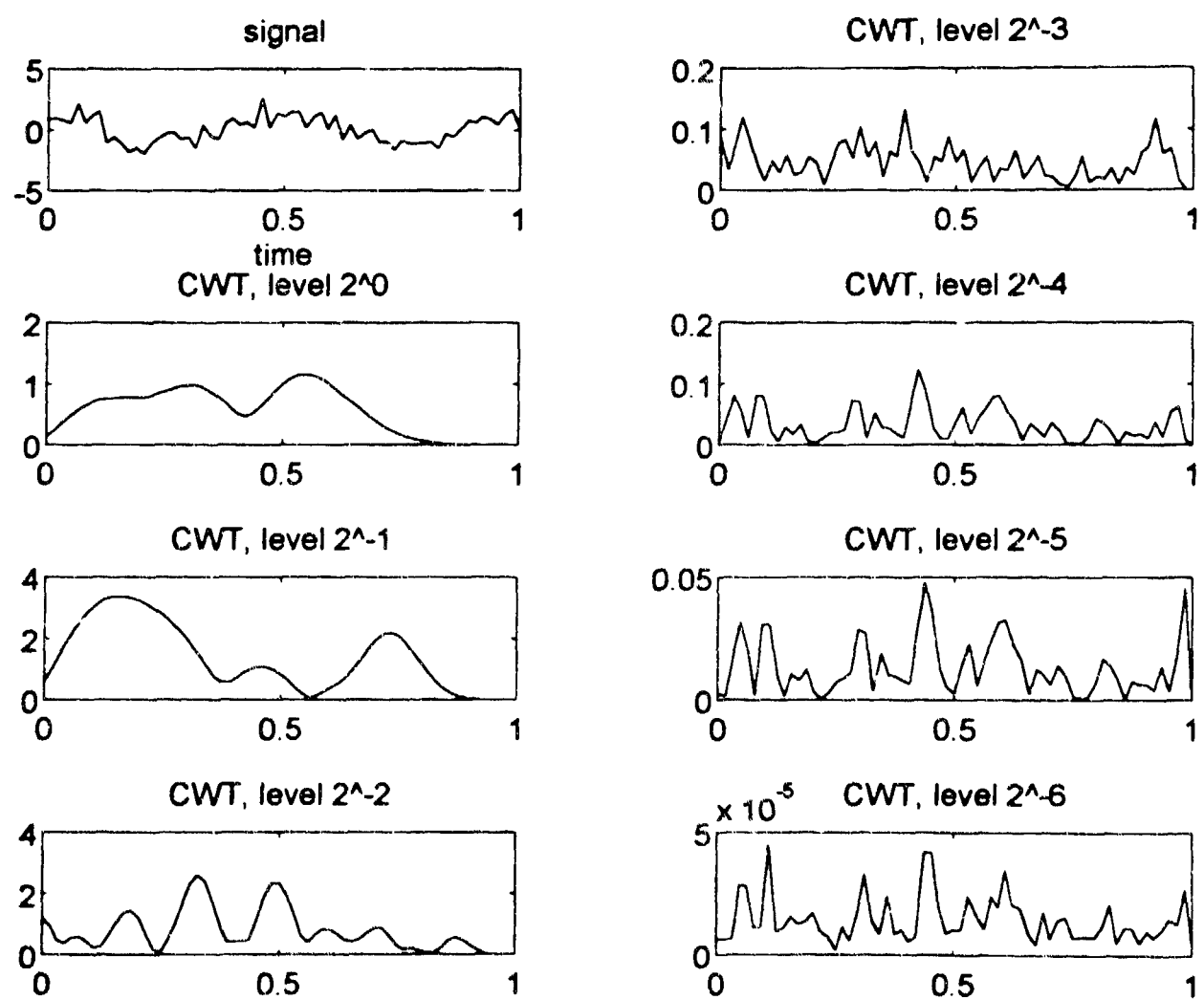


Figure 4.5 Magnitude of CWT of rectangular wave with complex modulated Gaussian wavelet. $\sigma = 0.12$, $f_\psi = 8$. SNR = 5 dB.

4.2 180° phase shift

The signal to be analyzed is now changed to a sinusoid with a 180° phase shift at $t = 0$, as shown in the first subplot of Figure 4.6. We use the Haar, Daubechies 10-coefficient, and the complex modulated Gaussian wavelets to analyze this signal and plot their CWTs in Figures 4.6, 4.7, and 4.8, respectively. For the Haar wavelet, the phase change also appears as a phase change in most of the CWTs as shown in Figure 4.6. The Daubechies wavelet does a better job in identifying the phase change, as shown in Figure 4.7. The complex modulated Gaussian wavelet also reveals clearly the phase shift in the magnitude plots of the CWT at $m = 4$ and $m = 5$, in addition a phase change is confirmed by $m = 1$ and $m = 2$ plots, as shown in Figure 4.8.

When there is noise, we found that both the Haar and Daubechies wavelets failed to perform.

When $\text{SNR} = 10$ dB (note that the signal power is equal to 0.5), we choose $\sigma = 0.12$ and $f_\psi = 12$ for the complex modulated Gaussian and show the magnitude and phase plots in Figures 4.9.a and 4.9.b. In Figure 4.9.a, the magnitude plot of the CWT at $m = 2$ reveals a phase shift activity somewhere on or before $t = 0.5$. (Note that there is an end-effect in the DWT due to finite signal window.) But the rest of the magnitude plots fail to pinpoint a better time location. When we consult the phase plots as shown in Figure 4.9.b, the $m = 6$ plot suggests that there is an abrupt change of phase at $t = 0.5$. This is confirmed by the $m = 3$ and $m = 6$ phase plots in Figure 4.9.c, where we use a different $f_\psi = 16$.

When $\text{SNR} = 5$ dB, we choose $\sigma = 0.12$, $f_\psi = 8$. The magnitude subplot for $m = 2$ of Figure 4.10.a reveals some phase activities; however, the other magnitude subplots and the phase plots of Figure 4.10.b yield no confirmative information. Detection of a single phase shift is very sensitive to the noise. However, when the signal window is much longer and more phase shifts are present, the complex modulated Gaussian would perform due to a larger output signal-power to noise power ratio (SNR_o , see (4.2)).

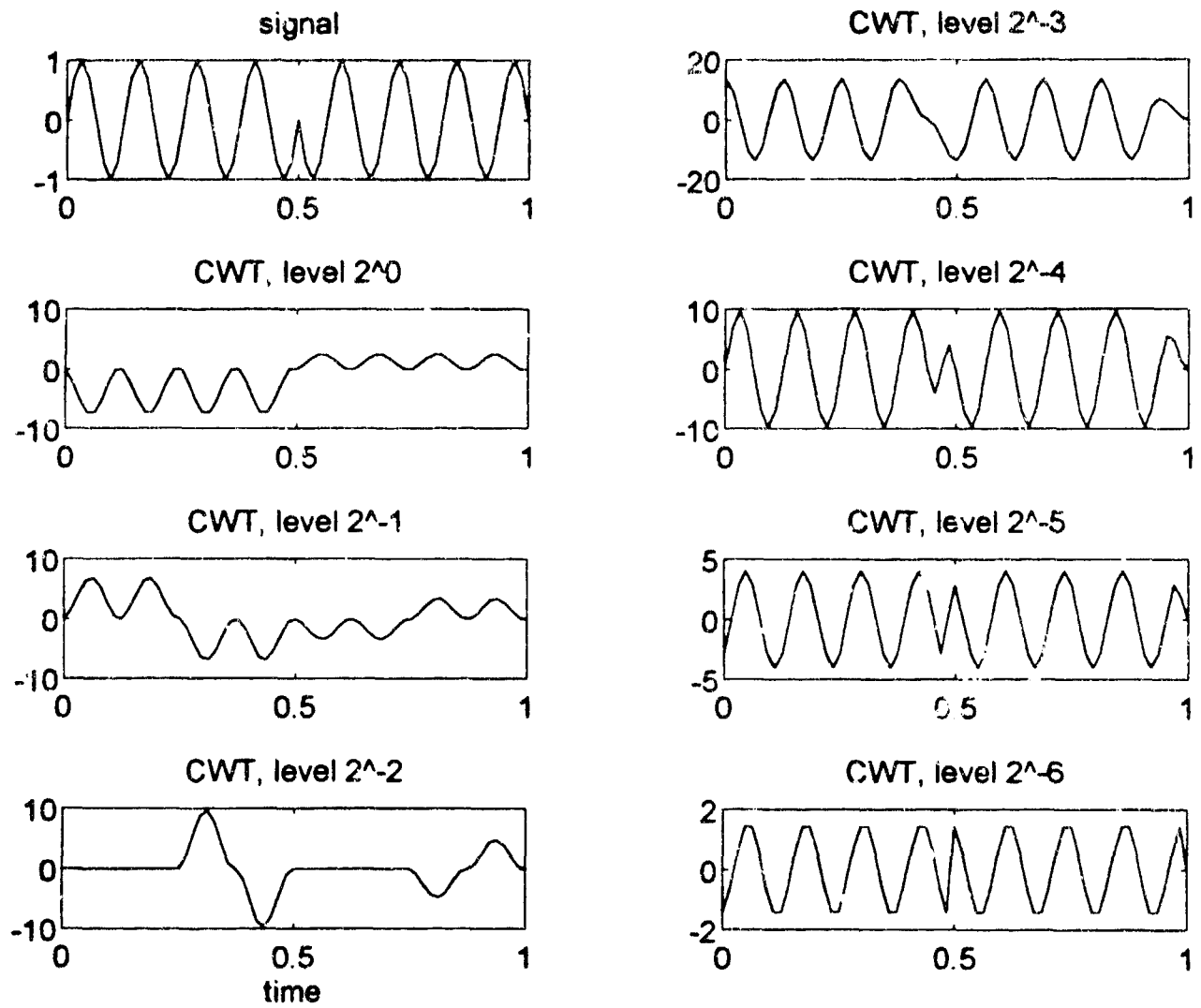


Figure 4.6 Magnitude of CWT of 180° phase shifted sinusoid with Haar wavelet. No noise.

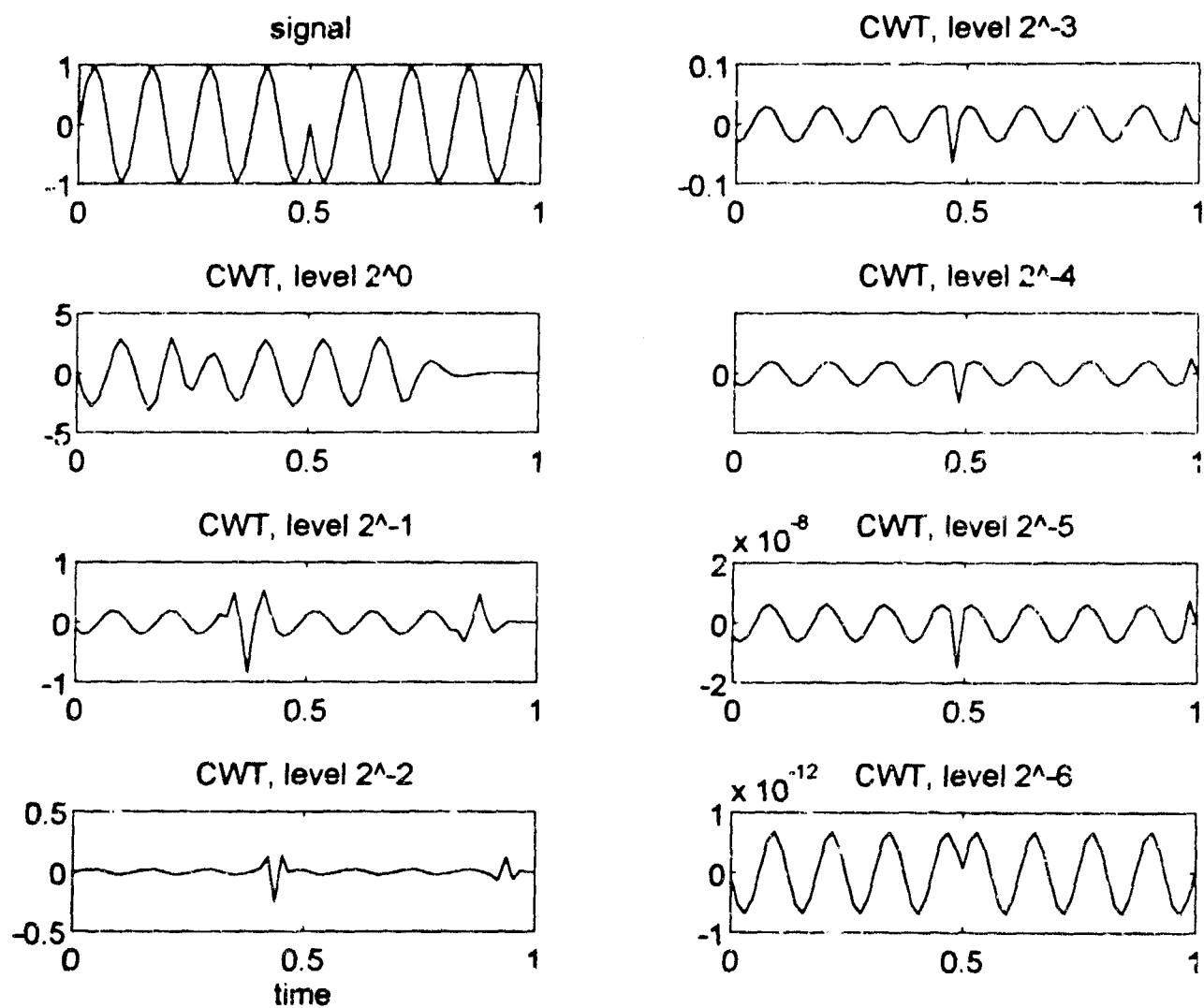


Figure 4.7 Magnitude of CWT of 180° phase shifted sinusoid with Daubechies 10-coefficient wavelet. No noise.

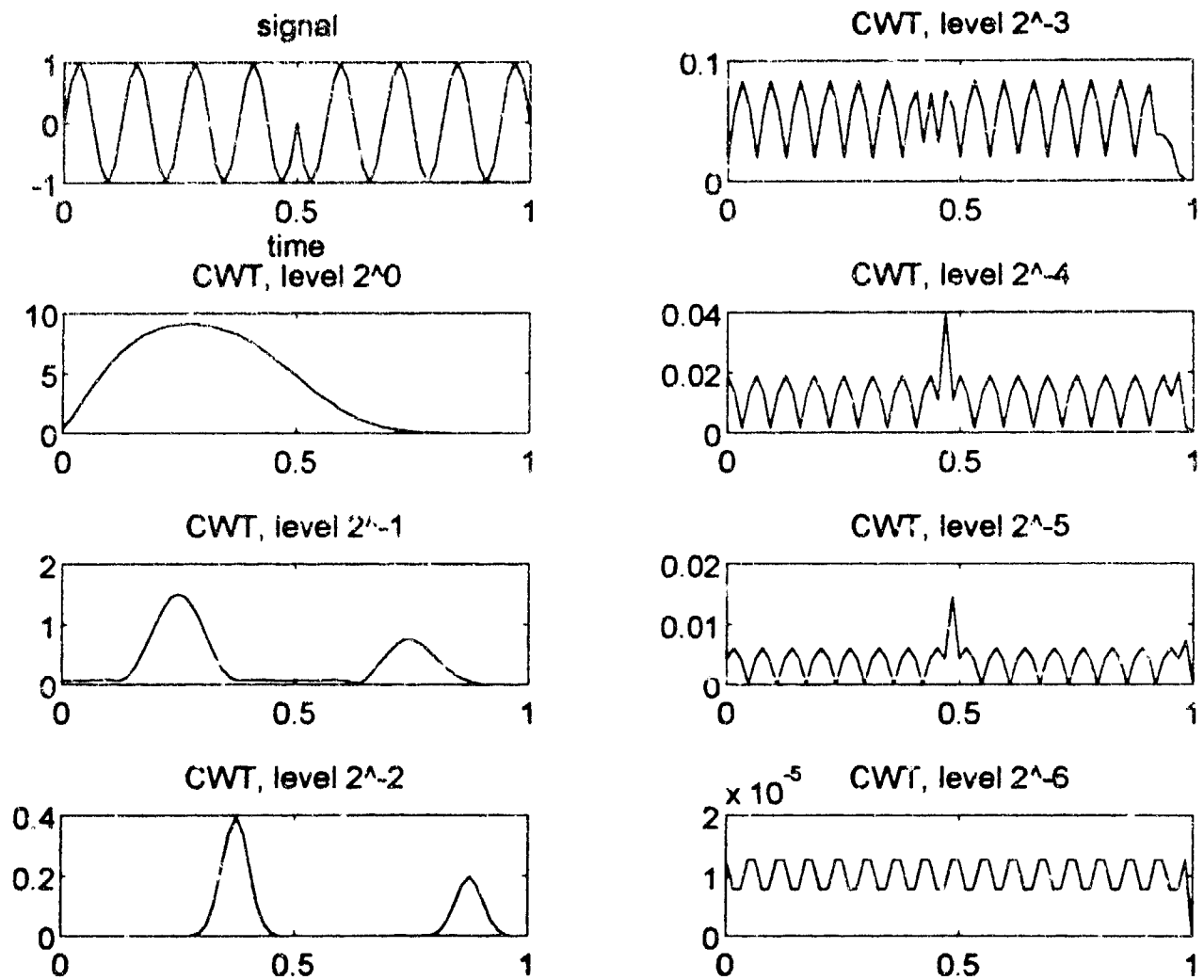


Figure 4.8 Magnitude of CWT of 180° phase shifted sinusoid with complex modulated Gaussian wavelet. $\sigma = 0.12$, $f_\psi = 8$. No noise.

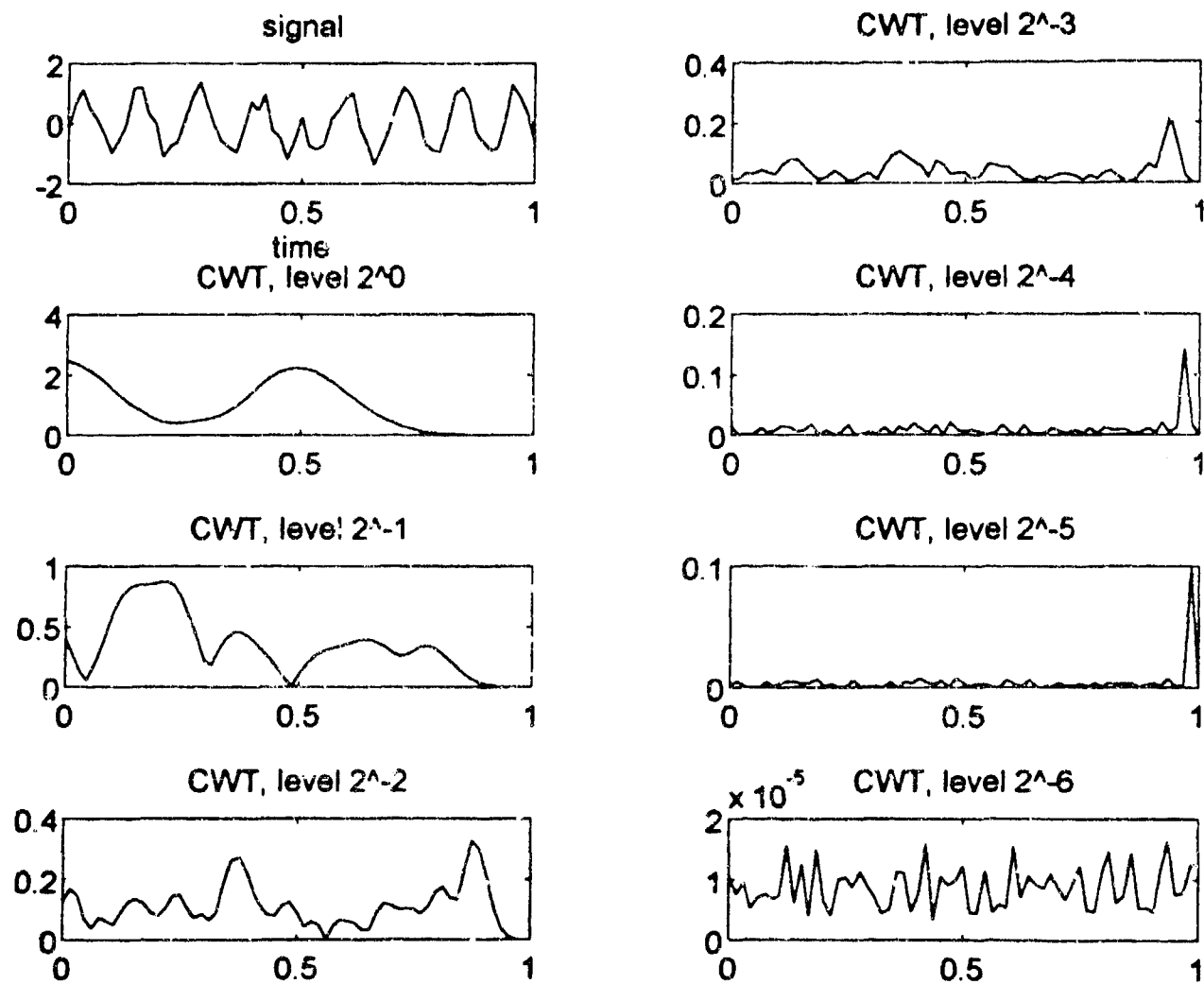


Figure 4.9.a Magnitude of CWT of 180° phase shifted sinusoid with complex modulated Gaussian wavelet. $\sigma = 0.12$, $f_{\psi} = 12$. SNR = 10 dB.

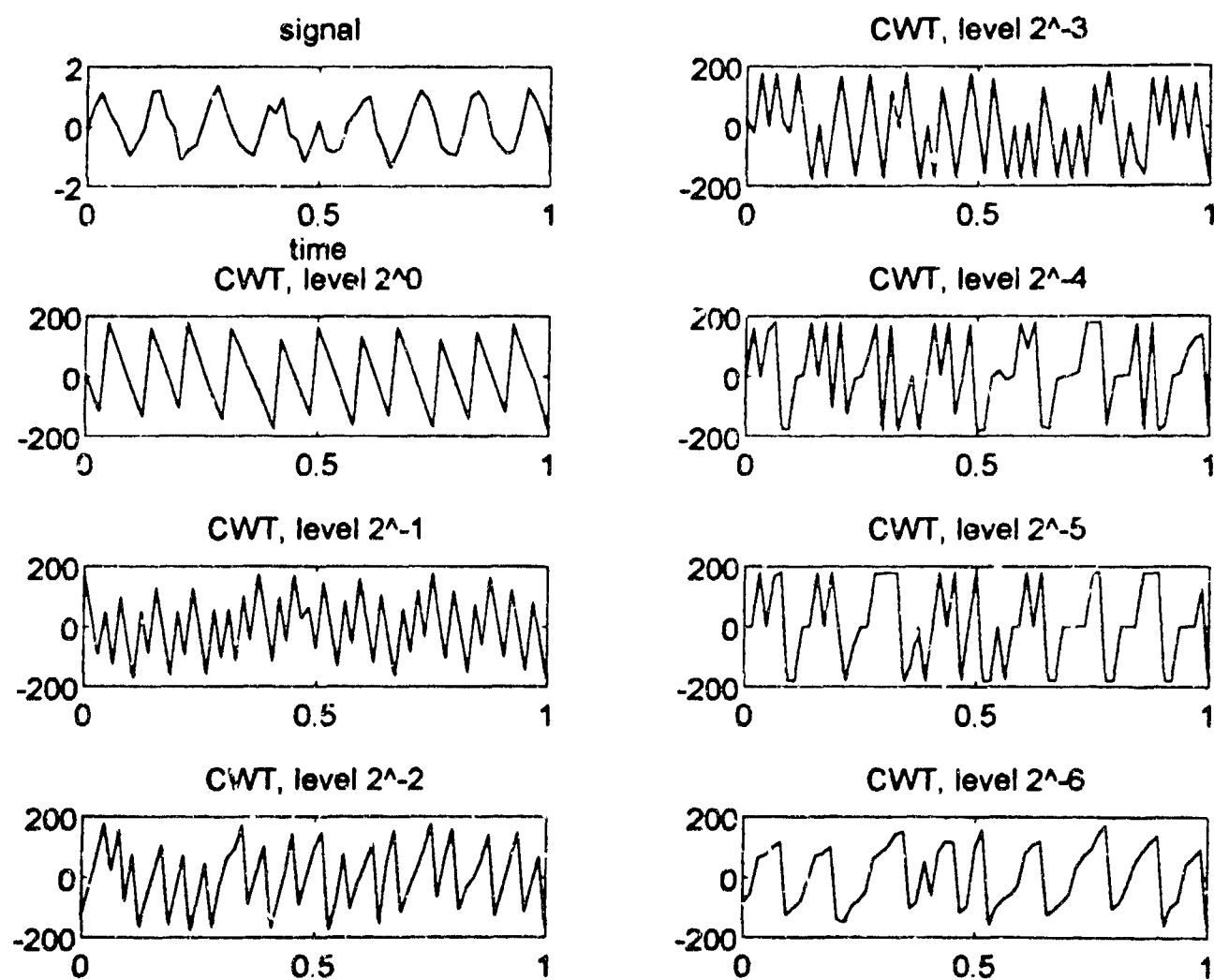


Figure 4.9.b Phase of CWT of 180° phase shifted sinusoid with complex modulated Gaussian wavelet. $\sigma = 0.12$, $f_{\psi} = 12$. SNR = 10 dB.

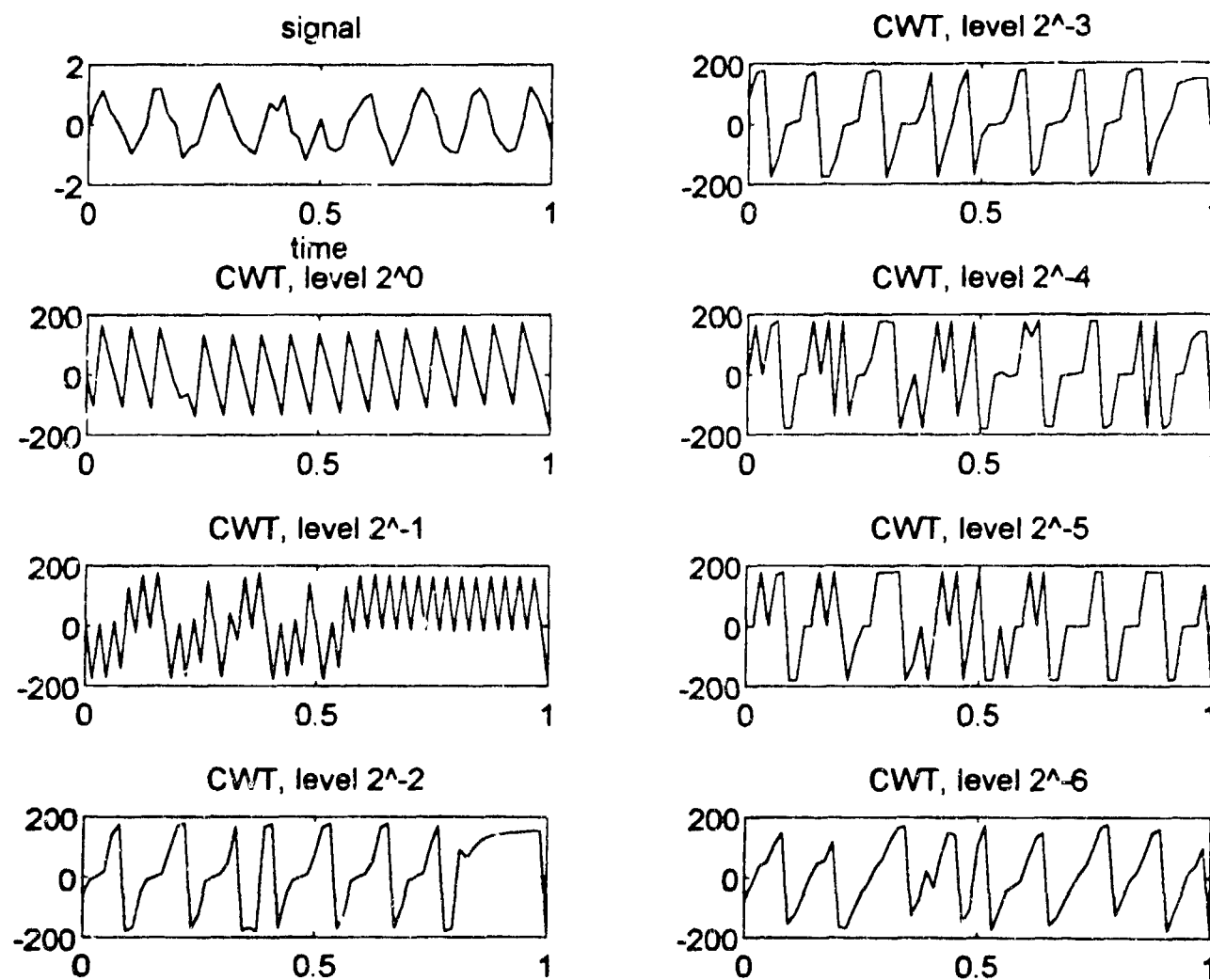


Figure 4.9.c Phase of CWT of 180° phase shifted sinusoid with complex modulated Gaussian wavelet. $\sigma = 0.12$, $f_{\psi} = 16$. SNR = 10 dB.

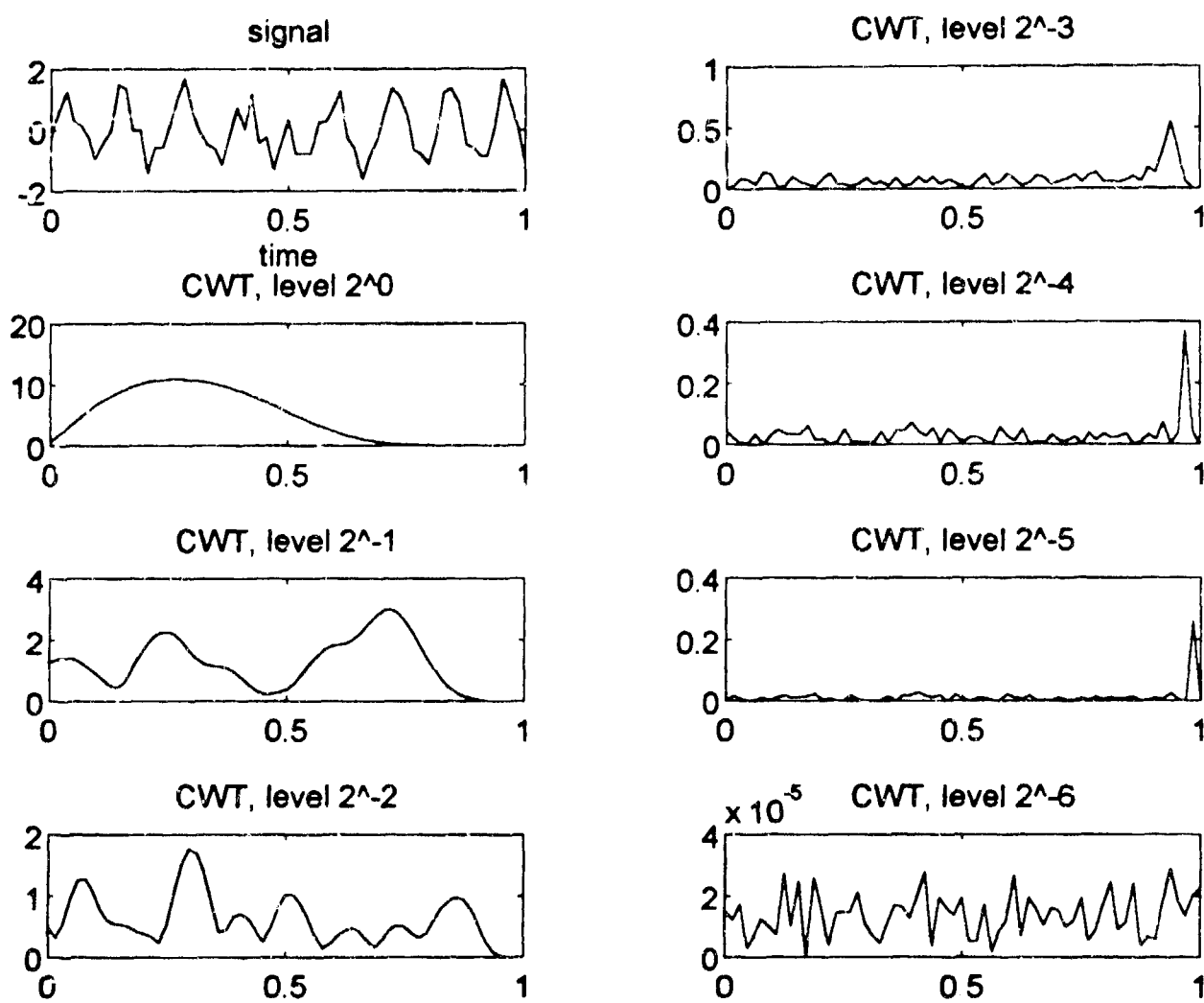


Figure 4.10.a Magnitude of CWT of 180° phase shifted sinusoid with complex modulated Gaussian wavelet. $\sigma = 0.12$, $f_{\psi} = 8$. SNR = 5 dB.

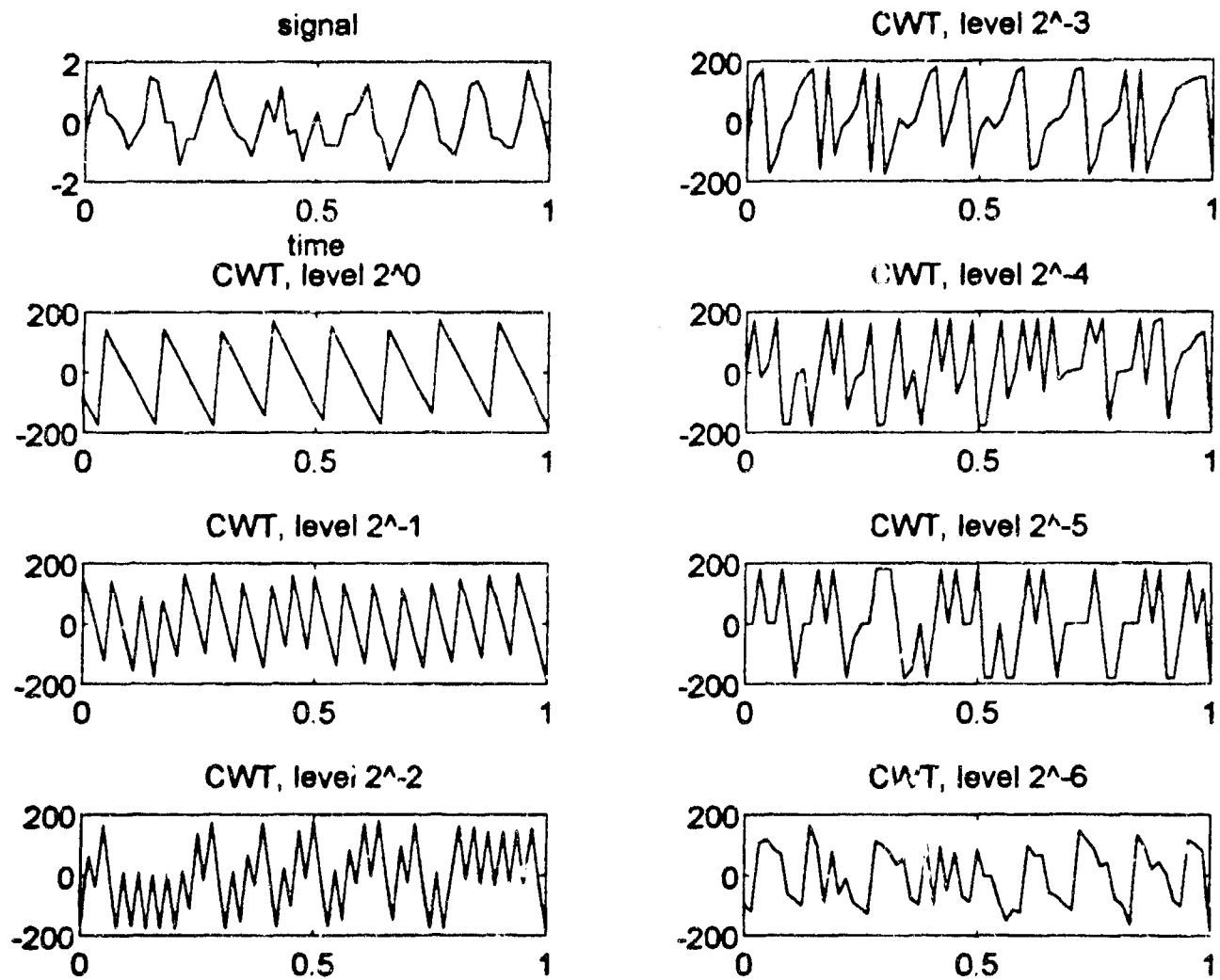


Figure 4.10.b Phase of CWT of 180° phase shifted sinusoid with complex modulated Gaussian wavelet. $\sigma = 0.12$, $f_p = 8$. SNR = 5 dB.

5. CONCLUDING REMARKS

Wavelet decompositions have better time-resolution at higher frequencies. They have better frequency-resolution at lower frequencies. Wavelet decompositions are suitable for analyzing signals that have high-frequency short pulses and/or low-frequency long pulses. The discrete wavelet transform (DWT) is primarily useful for data compaction, although we have found some of its potentials in signal detection. The continuous wavelet transform (CWT) can be used in signal detection. We have shown that by using complex modulated Gaussian wavelets, the time and frequency features of a signal can be revealed via a tunable, variable-bandwidth, multiresolution analysis. We have shown that CWT can be used in detecting PSK signals. However, the performance is sensitive to the level of noise.

REFERENCES

- [1] L. Cohen, "Time-frequency distributions—A review," *Proc. of the IEEE*, vol. 77, no. 7, pp. 941–981, July 1989.
- [2] I. Daubechies, "Orthonormal bases of compactly supported wavelets," *Comm. Pure and Appl. Math.*, vol. 41, pp. 909–996, 1988.
- [3] I. Daubechies, "The wavelet transform, time-frequency localization and signal analysis," *IEEE Trans. Info. Theory*, vol. 36, no. 5, pp. 961–1005, Sept. 1990.
- [4] L. E. Franks, unpublished notes on wavelets.
- [5] B. Friedlander and B. Porat, "Detection of transient signals by the Gabor representation," *IEEE Trans. ASSP.*, vol. 37, no. 2, pp. 169–180, Feb. 1989.
- [6] W. A. Gardner, "Signal interception: A unifying theoretical framework for feature detection," *IEEE Trans. Commun.*, vol. 36, no. 8, Aug. 1988.
- [7] M. J. Genossar, M. Goldberg, H. Lev-Ari, and T. Kailath, "Extending the wavelet decompositions to random processes with applications to periodically correlated processes," submitted.
- [8] A. Grossman and J. Morlet, "Decomposition of Hardy functions into square integrable wavelets of constant shape," *SIAM J. Math.*, vol. 15, pp. 723–736, 1984.
- [9] F. Hlawatsch and G. F. Boudreaux-Bartels, "Linear and quadratic time-frequency signal representations," *IEEE Sig. Proc. Magazine*, pp. 21–67, April 1992.
- [10] Mark Kalmbach, "Wavelet-based multiresolution analyses of signals", M.S. thesis, ECE, U.S. Naval Postgraduate School, June 1992. Advisor: A. W. Lam.
- [11] A. W. Lam and S. Tantarana, *Theory and Applications of Spread Spectrum*, IEEE Press, Sept. 1994.
- [12] A. W. Lam, "Spectrum of wavelet-decomposed random processes," *Proceedings of the 1991 Conference on Information Sciences and Systems*, pp. 896–901, Johns Hopkins University, March 1991.
- [13] A. W. Lam, "Time-frequency analysis of signals and systems," ECE, NPS, Monterey CA, interim reports, Sept 1993, Nov. 1993, April 1994.
- [14] Joey Legaspi, "One and two dimensional discrete wavelet transform", M.S. thesis, ECE, U.S. Naval Postgraduate School, Sept. 1992. Advisor: A. W. Lam.
- [15] S. G. Mallat, "A theory for multiresolution signal decomposition: The wavelet representation," *IEEE Trans. Pattern Analysis Machine Intelligence*, vol. 11, no. 7, pp. 674–693, July 1989.
- [16] S. G. Mallat, "Multiresolution approximations and wavelet orthonormal bases of $L^2(\mathbb{R})$," *Trans. American Math. Soc.*, vol. 315, no. 1, pp. 69–87, Sept. 1989.

- [17] S. G. Mallat, "Multifrequency channel decompositions of images and wavelet models," *IEEE Trans. ASSP*, vol. 37, no. 12, pp. 2091-2110, Dec. 1989.
- [18] S. G. Mallat, "Dyadic wavelet energy zero-crossings," *IEEE Trans. Info. Theory*, Jan. 1992.
- [19] D. Pollen, "Parametrization of compactly supported wavelets," AD890503.1.4, Aware, Inc., May 1989.
- [20] O. Rioul and M. Vetterli, "Wavelets and signal processing," *IEEE Sig. Proc. Magazine*, pp. 14-38, Oct. 1991.
- [21] R. O. Wells, Jr., "Parametrizing smooth compactly supported wavelets," AD891231, Aware, Inc., Dec. 1989.
- [22] G. W. Wornell, "A Karhunen-Loeve like expansion for $1/f$ processes via wavelets," *IEEE Trans. Info. Theory*, vol. 36, no. 4, pp. 859-861, July 1990.
- [23] Y. Zhao, L. E. Atlas, and R. J. Marks, II, "The use of cone-shaped kernels for generalized time-frequency representations of nonstationary signals," *IEEE Trans. ASSP*, vol. 38, no. 7, pp. 1084-1091, July 1990.

INITIAL DISTRIBUTION LIST

	No. Copies
1. Defense Technical Information Center Cameron Station Alexandria, VA 22304-6145	2
2. Dudley Knox Library, Code 52 Naval Postgraduate School Monterey, CA 93943-5002	2
3. Chairman, Code EC Department of Electrical and Computer Engineering Naval Postgraduate School 833 Dyer Road, Room 437 Monterey, CA 93943-5121	1
4. Professor A. W. Lam, Code EC/La Department of Electrical and Computer Engineering Naval Postgraduate School Monterey, CA 93943-0000	5
5. Professor Herschel H. Ioomis, Code EC/Lm Department of Electrical and Computer Engineering Naval Postgraduate School Monterey, CA 93943-5000	1